

ABSTRACT

Thielemier, Maxwell. Impact and Spread Characteristics of Kerosene Gelled with Fumed Silica (Under the direction of Dr. Tiegang Fang).

Gelled fuels have been studied extensively due to their beneficial properties both in functionality and storage. These gels are formed by combining a gelling agent, either organic or inorganic, with an appropriate fuel of choice. They are shear thinning and thus behave like a solid at rest and a liquid while under the effects of shear. This allows the gels to be pumped through fuel lines and atomized while maintaining safety during rest and transportation. This increased safety comes from high viscosity which prevents sloshing in containers and decreases leaking that may occur.

Although it is understood that gelled fuels provide better safety standards, this area has not been well explored through literature. This brings into question how to quantify the safety of these gels and whether the safety benefits of these gels are worth the difficulty it takes to atomize them. The main purpose of this paper is to quantify the safety of these gels under different scenarios through measuring the spread area of individual droplets onto various materials. However, the results from these tests have applications in a range of systems such as fuel pumps, combustion chamber walls, and anywhere else the fuel droplets may come into contact with surfaces.

The parameters being examined are the Weber number, changed by altering the droplet height, the gellant concentration, and material being impacted. The fuel being used is Crown 1-K Kerosene gelled with fumed silica in concentrations ranging from 2wt% to 6wt%. This gelled fuel shows promising results for decreasing the spread area particularly with higher gelling percentages.

© Copyright 2023 by Maxwell Thielemier

All Rights Reserved

Impact and Spread Characteristics of Kerosene Gelled with Fumed Silica.

by
Maxwell Thielemier

A thesis submitted to the Graduate Faculty of
North Carolina State University
in partial fulfillment of the
requirements for the degree of
Master of Science

Aerospace Engineering

Raleigh, North Carolina
2023

APPROVED BY:

Dr. Tiegang Fang
Committee Chair

Dr. Arun Kumar Kota

Dr. Hooman Tafreshi

DEDICATION

Dedicated to my parents who have believed in me every step of the way.

BIOGRAPHY

Maxwell Curtis Thielemier was born in the year 1999 in Memphis, TN. After playing with too many Legos he quickly became infatuated with the ideas of engineering leading to a five-year stint at space camp. Through these experiences he became intrigued with understanding the fundamental mechanisms of our universe. After graduating high school in 2017, Max went on to study physics at Loyola University of Chicago and developed a deeper understanding of other topics as well such as music and mathematics. He graduated with an undergraduate degree in 2021 and decided to continue working towards a higher education. Turning away from the theoretical side towards the practical, Max went on to pursue a Master of Science in Aerospace Engineering from North Carolina State University. Here, he studied a variety of engineering topics and joined the research group of Dr. Tiegang Fang in 2022 after learning about the exciting research being done there.

ACKNOWLEDGMENTS

I would like to express my appreciation towards my thesis advisor Dr. Tiegang Fang for helping me make the most of this great opportunity. I could not imagine a more fitting research professor. Along with this, thank you to the professors who have helped me along the way including Dr. Saad Khan who helped me with rheology data and Dr. Gracious Ngaile who allowed me to access equipment for measuring surface roughness as well as the two other members of my thesis committee, Dr. Arun Kumar Kota and Dr. Hooman Tafreshi. Additionally, I would not have been able to get this far without the help of the fellow members of Dr. Fang's research group, Kaushik Nonavinakere Vinod, Nigel Liu, Matt Gore, Vibhav Vidyadhar, Charlie Drew, Robert Kempin, Ryan Abell, and Caleb Kebede. The input and assistance they provided was pivotal in the completion of this research. Of course, I would not be here without the love and support from my parents and family members.

TABLE OF CONTENTS

LIST OF TABLES	vi
LIST OF FIGURES	vii
Chapter 1: Introduction	1
Chapter 2: Experimental Preparation	7
2.1 Experimental setup.....	7
2.2 Gel formulation and properties	9
2.3 Weber number calculations.....	18
Chapter 3: Results and Discussion	19
3.1 Effect of gellant percentage	19
3.2 Changing Weber number	23
3.3 Different surface effects.....	28
3.3.1 Aluminum	28
3.3.2 Nickel.....	35
3.3.3 Stainless steel	42
3.3.4 Smooth oleophobic glass	49
3.4 Next steps.....	56
Chapter 4: Conclusion	58
References	59

LIST OF TABLES

Table 2.1	Properties of the gels used in the impact experiments	12
Table 2.2	The length of the pendant, heigh, and width of the droplet for each gel.....	17
Table 3.1	Impact characteristics from 50cm onto smooth glass	23
Table 3.2	Impact characteristics from 100cm onto smooth glass	26
Table 3.3	Impact characteristics from 50cm onto aluminum	33
Table 3.4	Impact characteristics from 100cm onto aluminum	34
Table 3.5	Impact characteristics from 50cm onto nickel	40
Table 3.6	Impact characteristics from 100cm onto nickel	41
Table 3.7	Impact characteristics from 50cm onto stainless steel	47
Table 3.8	Impact characteristics from 100cm onto stainless steel	48
Table 3.9	Impact characteristics from 50cm onto smooth oleophobic glass.....	54
Table 3.10	Impact characteristics from 100cm onto smooth oleophobic glass.....	55

LIST OF FIGURES

Figure 1.1 Gel fuel research areas from Padwel (2021)	2
Figure 1.2 (a) gelled kerosene with boron, (b) gelled kerosene, (c) gelled kerosene with aluminum, and (d) kerosene from Yang (2001)	4
Figure 1.3 The six possible impact regimes occurring at different Weber numbers from Jadidbonab (2018)	6
Figure 2.1 Droplet experiment setup	8
Figure 2.2 Separated kerosene gelled with 6wt% of fumed silica	10
Figure 2.3 Kerosene gelled with a range of 2wt% (left) to 6wt% (right) of fumed silica	11
Figure 2.4 Rheological Profile of the 2wt% Gel.....	13
Figure 2.5 Rheological Profile of the 3wt% Gel.....	13
Figure 2.6 Rheological Profile of the 4wt% Gel.....	13
Figure 2.7 Rheological Profile of the 5wt% Gel.....	14
Figure 2.8 Rheological Profile of the 6wt% Gel.....	14
Figure 2.9 0wt% droplet formation and freefall	15
Figure 2.10 1wt% droplet formation and freefall	15
Figure 2.11 2wt% droplet formation and freefall	15
Figure 2.12 3wt% droplet formation and freefall	16
Figure 2.13 4wt% droplet formation and freefall	16
Figure 2.14 5wt% droplet formation and freefall	16
Figure 2.15 6wt% droplet formation and freefall	16
Figure 3.1 0wt% impact onto smooth glass from 50cm.	19
Figure 3.2 2wt% impact onto smooth glass from 50cm.	20
Figure 3.3 4wt% impact onto smooth glass from 50cm.	20

Figure 3.4	6wt% impact onto smooth glass from 50cm.	21
Figure 3.5	Spread comparison from 50cm onto smooth glass for 0wt% (left) to 6wt% (right).....	22
Figure 3.6	0wt% impact onto smooth glass from 100cm.	24
Figure 3.7	2wt% impact onto smooth glass from 100cm.	24
Figure 3.8	4wt% impact onto smooth glass from 100cm.	25
Figure 3.9	6wt% impact onto smooth glass from 100cm.	25
Figure 3.10	Spread comparison from 100cm onto smooth glass for 0wt% (left) to 6wt% (right).....	26
Figure 3.11	The spread diameter over time for each impact onto the smooth glass.....	28
Figure 3.12	0wt% impact onto aluminum from 50cm.....	29
Figure 3.13	0wt% impact onto aluminum from 100cm.....	29
Figure 3.14	2wt% impact onto aluminum from 50cm.....	30
Figure 3.15	2wt% impact onto aluminum from 100cm.....	30
Figure 3.16	4wt% impact onto aluminum from 50cm.....	31
Figure 3.17	4wt% impact onto aluminum from 100cm.....	31
Figure 3.18	6wt% impact onto aluminum from 50cm.....	32
Figure 3.19	6wt% impact onto aluminum from 100cm.....	32
Figure 3.20	Spread comparison from 50cm onto aluminum for 0wt% (left) to 6wt% (right).....	33
Figure 3.21	Spread comparison from 100cm onto aluminum for 0wt% (left) to 6wt% (right).....	33
Figure 3.22	The spread diameter over time for each impact onto the aluminum	35
Figure 3.23	0wt% impact onto nickel from 50cm.	36
Figure 3.24	0wt% impact onto nickel from 100cm.	36

Figure 3.25 2wt% impact onto nickel from 50cm.	37
Figure 3.26 2wt% impact onto nickel from 100cm.	37
Figure 3.27 4wt% impact onto nickel from 50cm.	38
Figure 3.28 4wt% impact onto nickel from 100cm.	38
Figure 3.29 6wt% impact onto nickel from 50cm.	39
Figure 3.30 6wt% impact onto nickel from 100cm.	39
Figure 3.31 Spread comparison from 50cm onto nickel for 0wt% (left) to 6wt% (right).....	40
Figure 3.32 Spread comparison from 100cm onto nickel for 0wt% (left) to 6wt% (right).....	40
Figure 3.33 The spread diameter over time for each impact onto nickel	42
Figure 3.34 0wt% impact onto stainless steel from 50cm.	43
Figure 3.35 0wt% impact onto stainless steel from 100cm.	43
Figure 3.36 2wt% impact onto stainless steel from 50cm.	44
Figure 3.37 2wt% impact onto stainless steel from 100cm.	44
Figure 3.38 4wt% impact onto stainless steel from 50cm.	45
Figure 3.39 4wt% impact onto stainless steel from 100cm.	45
Figure 3.40 6wt% impact onto stainless steel from 50cm.	46
Figure 3.41 6wt% impact onto stainless steel from 100cm.	46
Figure 3.42 Spread comparison from 50cm onto stainless steel for 0wt% (left) to 6wt% (right).....	47
Figure 3.43 Spread comparison from 100cm onto stainless steel for 0wt% (left) to 6wt% (right).....	47
Figure 3.44 The spread diameter over time for each impact onto stainless steel	49
Figure 3.45 0wt% impact onto smooth oleophobic glass from 50cm.	50

Figure 3.46 0wt% impact onto smooth oleophobic glass from 100cm.	50
Figure 3.47 2wt% impact onto smooth oleophobic glass from 50cm.	51
Figure 3.48 2wt% impact onto smooth oleophobic glass from 100cm.	51
Figure 3.49 4wt% impact onto smooth oleophobic glass from 50cm.	52
Figure 3.50 4wt% impact onto smooth oleophobic glass from 100cm.	52
Figure 3.51 6wt% impact onto smooth oleophobic glass from 50cm.	53
Figure 3.52 6wt% impact onto smooth oleophobic glass from 100cm.	53
Figure 3.53 Spread comparison from 50cm onto smooth oleophobic glass for 0wt% (left) to 6wt% (right).....	54
Figure 3.54 Spread comparison from 100cm onto smooth oleophobic glass for 0wt% (left) to 6wt% (right).....	54
Figure 3.55 The spread diameter over time for each impact onto oleophobic glass	56

CHAPTER 1

INTRODUCTION

Padwal et al. (2021) gives a detailed overview of the history of the usage and development of gelled fuels. These gel fuels are almost always functionally similar to liquid fuels in that they are pumped through an atomizer before combustion but have a much higher viscosity when not applied with shear and thus behave like solids at rest. This comes with a variety of advantages over liquid and solid fuel including a higher specific impulse and density impulse, reduced leakage, reduced weight, and less sloshing. These are formulated by adding a gelling agent to a typical liquid fuel to produce a shear thinning gel. There are a wide variety of gelling agents used but they can be separated into two categories, organic and inorganic. Organic gelling agents burn up along with the fuel they are mixed with, but inorganic gelling agents remain in a solid state after combustion. Like solid fuels, they can also support the suspension of metal particles to achieve benefits in energy density. However, these gelled fuels come with a variety of disadvantages as well such as being difficult to atomize, unable to reach very low viscosities, requiring higher pressure changes, and longer burn time among others. These gels have proven difficult to implement as fuel in ramjets due to the level of atomization required to achieve ignition in a short time frame. However, improvements in atomizers have been able to produce a low enough particle diameter for some gelled fuels to function in ramjets although inhomogeneity of the fuel mixture may have an effect. Generally, these gelled fuels offer good theoretical performance but are difficult to implement compared to liquid and solid fuels. Padwal gives a good summary of the research areas revolving around gelled fuels in Figure 1.1.

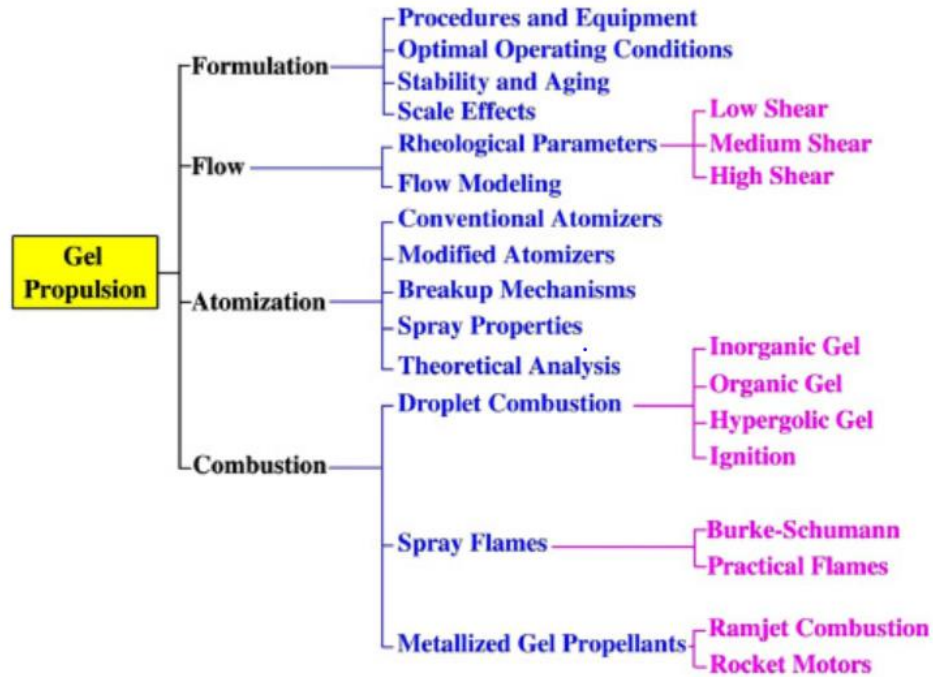


Figure 1.1: Gel fuel research areas from Padwel (2021).

Li et al. (2022b) studied the rheological properties of kerosene gelled with the organic gelling agent THIXATROL ST and developed a model to predict the viscosity of these gels at different temperatures and shear rates. They formulated gels from 4wt% to 6wt% of gelling agent and thoroughly investigated their rheological properties. Other than the expected results of a shear thinning gel, they found that the shear history has a strong effect on the current viscosity of the gels. For instance, a pre-sheared gel displayed much lower viscosities under low shear rates than the same gel without pre-shearing. They found that after this pre-shearing has occurred, the rheological curve can be approximated by a power law relationship in which the power law exponent n remains constant, and the consistency coefficient K increases along with the gellant percentage.

The work done by Padwal and Mishra (2013) lays out the groundwork for the successful formulation of gelled Jet A1 fuel using an organic gelling agent. They focused on analyzing

separation tendencies as a result of processing temperatures as well as attempts at atomizing the gels. They found that the minimum gelling agent required to produce a gel was 2.22wt% while the gels above 5wt% exhibit no phase separation. These results were interesting as the minimum concentration of gelling agent required for the gels used in this paper is between 1wt% and 2wt% of fumed silica.

An important property used in many of the calculations in this paper is the surface tension, which becomes more difficult to determine as the gellant percentage increases. To explore the measurement of surface tension for highly elastic fluids, Jørgensen et al. (2015) performed a variety of surface tension measurements on different Carbopol gels. Their main analysis involved the use of a bridge tensiometer which determines the surface tension force of a fluid between two close together plates. The liquid sticks to the bottom and the top plate forming a bridge between them which can be used to determine surface tension. They were able to receive accurate trends for the surface tension of the Carbopol gels but found that the resulting surface tension largely depends on the experimental method. For example, pre-shearing the gels in a particular direction during or before the measurement results in large discrepancies between data points for surface tension measurements. This outlines the difficulty of accurate surface tension measurements for fluids with viscoelastic properties.

As mentioned, gelled fuels can support the suspension of metal particles which may improve the energy density of the fuel. Li et al. (2022a) examined the properties of these metalized fuel gels under large scale oscillatory shearing to mimic pumping characteristics. They found that an increase in aluminum filler increased the energy dissipation of the gels while also increasing their plasticity. They go into detail on the different hardening and thinning behaviors resulting from associated unstable wave interfaces.

Additional analysis of metalized gels was performed by Yang et al. (2001). Here they formulated kerosene gelled with Polyamide Resin and loaded large amounts of either aluminum or boron to increase specific impulse density. They found that the gels can be loaded with up to 45wt% of metal particles and the boron suspension results in a much larger viscosity and surface tension than the similar aluminum loaded gels. Although the metals have a higher ignition temperature than the fuel, they were still able to achieve successful particle ignition. The gels formulated in the study are shown in Figure 1.2 inverted in their containers such that they cannot flow to the bottom. They also discussed the deformation characteristics of a suspended droplet with different gellant concentrations.

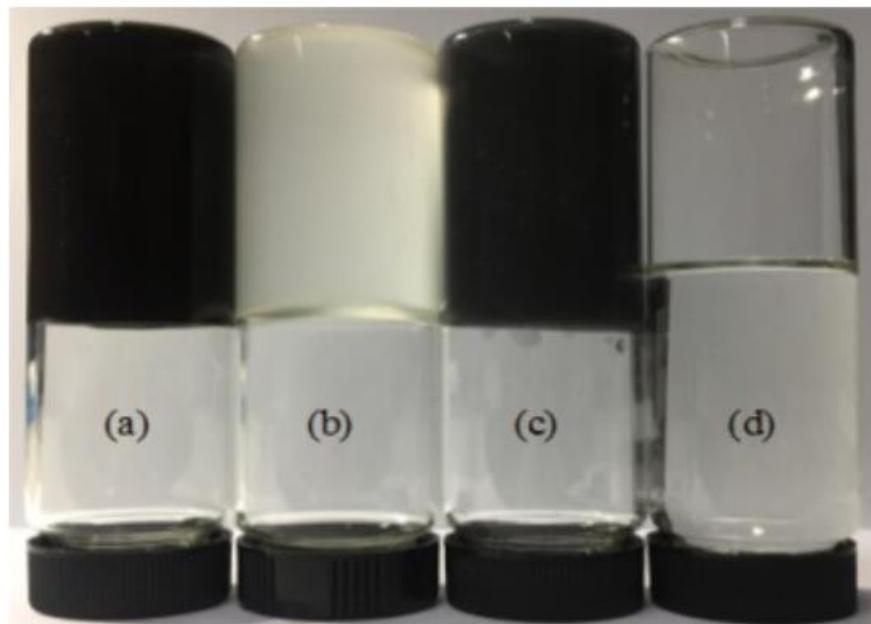


Figure 1.2: (a) gelled kerosene with boron, (b) gelled kerosene, (c) gelled kerosene with aluminum, and (d) kerosene from Yang (2001).

Numerical studies such as the one done by Cao et al. (2022) have analyzed the secondary atomization process of similar kerosene-based gels with fumed silica as the gelling agent. They demonstrated the breakup morphology of these gels at a range of weber numbers showing a transition from bag mode to multimode at higher Weber number values. They explain how the

Weber number measures the ratio of the resistant forces on a fluid over its surface tension. In other words, higher Weber numbers result in a higher likelihood of droplet breakup. Along with this, changes in Weber numbers affect the breakup morphology of the gels turning from bag mode to multimode as the Weber number increases. An additional, expected result is a decrease in breakup time as the Weber number is increased.

Another experiment performed by Cao et al. (2019) characterized the combustion morphology of kerosene gelled with various weight percentages of inorganic fumed silica compared to kerosene gelled with an organic gelling agent. The inorganic gels produced a rigid shell when burned that prevented expansion and contraction during ignition. This results in better combustion stability than the organic gels as well as a higher combustion rate at later stages. These results are optimistic for inorganic gellants as long as the unburnt residue can be properly expelled from the engine system.

Due to the wide variety of variables involved in droplet impact experiments, it is often difficult to predict the outcome. Wang et al. (2016) developed a numerical simulation that can predict many aspects of droplet impacts using the Reynolds and Ohnesorge numbers. Their simulation was compared with experimental results and was found to be accurately able to predict droplet impact outcomes including the spread area. They found that the early spreading characteristics are highly dependent on the fluid properties and the spreading time is generally unaffected by these properties unless the Weber number is less than one.

Research performed by Jadidbonab et al. (2018) explored and characterized the impact of diesel fuel droplets at a range of Weber and Reynolds numbers. They denoted key value pairs for the temperature and Weber number which change the characteristics of the impact regime. They

determined six possible impact regimes outlined in Figure 1.3 which are highly influenced by the Weber number at impact.

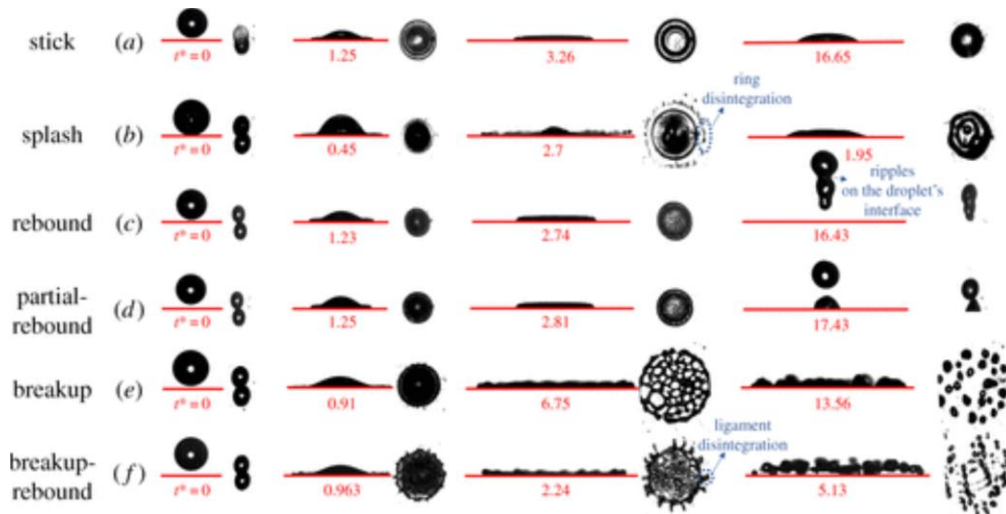


Figure 1.3: The six possible impact regimes occurring at different Weber numbers from Jadidbonab (2018).

One of the factors preventing a more widespread use of gelled fuels is their difficulty to spray and atomize. Fu et al. (2019) explored this with gelled propellant in a swirl injector. They found several interesting results including the increase in spray cone angle and a decrease in the breakup length as the pressure difference is increased. On the other hand, the breakup length increases with gellant concentration. This leads to a general relationship of higher gellant concentrations leading to higher pressure requirements for pumping through fuel injectors.

CHAPTER 2

EXPERIMENTAL PREPARATION

2.1 Experimental Setup

The experiments in this paper revolve around high-speed videos of gelled fuel droplets impacting different surfaces. The videos are recorded using a phantom high-speed camera with a 55mm lens located 19cm away from the impact and oriented to be level with the impact plate. The resolution is set to 256x256, the exposure time is 4 μ s, and the sample rate is 8146 fps. To provide contrast, a 30V light source and light diffuser are placed behind the droplet oriented towards the high-speed camera. A DSLR camera is placed above the impact to capture the spread characteristics. This camera is not looking directly down at the droplet but is instead offset by 28° which gives a good view of the impact zone without obstructing the droplets. The fluid is fed through a needle of inner diameter 1.372mm and outer diameter 1.829mm and placed a variable distance above the plate. The plate is level with the ground and several different materials are placed on the plate for impact analysis. The entire setup is shown in Figure 2.1.



Figure 2.1: Droplet experiment setup

Three different metals were chosen as impact surfaces due to their likelihood of coming into proximity with the fuel in propulsion systems. The surface roughness of the materials was measured with a Mitutoyo SJ-310 – Portable Surface Roughness Tester. These are aluminum (roughness $20.686\mu\text{in}$), nickel alloy 625 (roughness $3.476\mu\text{in}$), and stainless steel alloy 321 (roughness $5.688\mu\text{in}$). Two additional surfaces were analyzed, the first being smooth glass (roughness $0.146\mu\text{in}$) and the second is the same smooth glass with an oleophobic surface coating. The product used for the oleophobic coating is called Fusso and was purchased via Amazon. It is applied as a thin liquid layer which solidifies as each coat dries. Eight coats were applied over a series of five days which resulted in a semi oleophobic surface with interesting impact characteristics.

2.2 Gel Formulation and Properties

The fuels used in the droplet experiments performed in this paper consisted of Crown 1-K kerosene gelled with hydrophilic fumed silica. This results in a non-Newtonian, shear thinning gel. The fumed silica used here has a bulk density of 2.3lb/cu.ft at 25° C, a B.E.T surface area of 175-225 meters squared/g and an average particle size of 0.2-0.3 μ m. To produce the desired gels, the fumed silica was poured into the kerosene at room temperature and sheared with a magnetic stirrer for around thirty minutes. The thicker gels were shaken every few minutes to disperse the gelling agent evenly. This was done for 1wt%, 2wt%, 3wt%, 4wt%, 5wt%, and 6wt% of fumed silica with mixed results. In the 1wt% mixtures, the gelling agent failed to fully disperse itself through the kerosene and resulted in inhomogeneous mixtures. This was characterized by cloudy sections of the otherwise clear fluid which would settle to the bottom when left at rest. For this reason, the 1wt% gels are not further considered for the droplet experiments. Another issue that became apparent during the formulation of these gels is the likelihood of a poor yield. This would result in a gel that was much thinner than expected and has a higher tendency for separation. This can be seen in Figure 2.1 which shows a 6wt% gel that has been inverted to examine flow properties. The thin, less viscous layer flowing to the bottom while the highly viscous layer remaining on top is a clear indication of separation occurring in this gel. Poor yield can be caused by a variety of factors such as stirring speed and humidity levels contributing to the fumed silica not being fully wetted out.



Figure 2.2: Separated kerosene gelled with 6wt% of fumed silica.

Each gel was closely examined for separation tendencies and flow consistency and the best batches were moved forward for rheological analysis and droplet impact tests. An example of good quality gels is shown in Figure 2.3. These all exhibit consistency throughout the fluid with very little to no separation. A batch of gels was left at rest for a period of a month and no additional separation was observed although longer periods of observation are required to better examine the long-term stability of these gels. As we can see, the gels of 4wt% and below all flow of their own accord to the bottom of the container while the gels of 5wt% and higher remain suspended at the top. With this in consideration, the cutoff point for these gels flowing of their own accord is between 4wt% and 5wt%. Conveniently, this is also the point at which the gels can no longer form droplets. That is to say that the surface tension of the gels above 4% is no longer strong enough to form the gel into a sphere in freefall due to the increased viscosity of these gels preventing a change in shape. These also demonstrate the increase of density caused

by the addition of the gelling agent as each of these mixtures weighs 15 grams, but their volumes are all different.

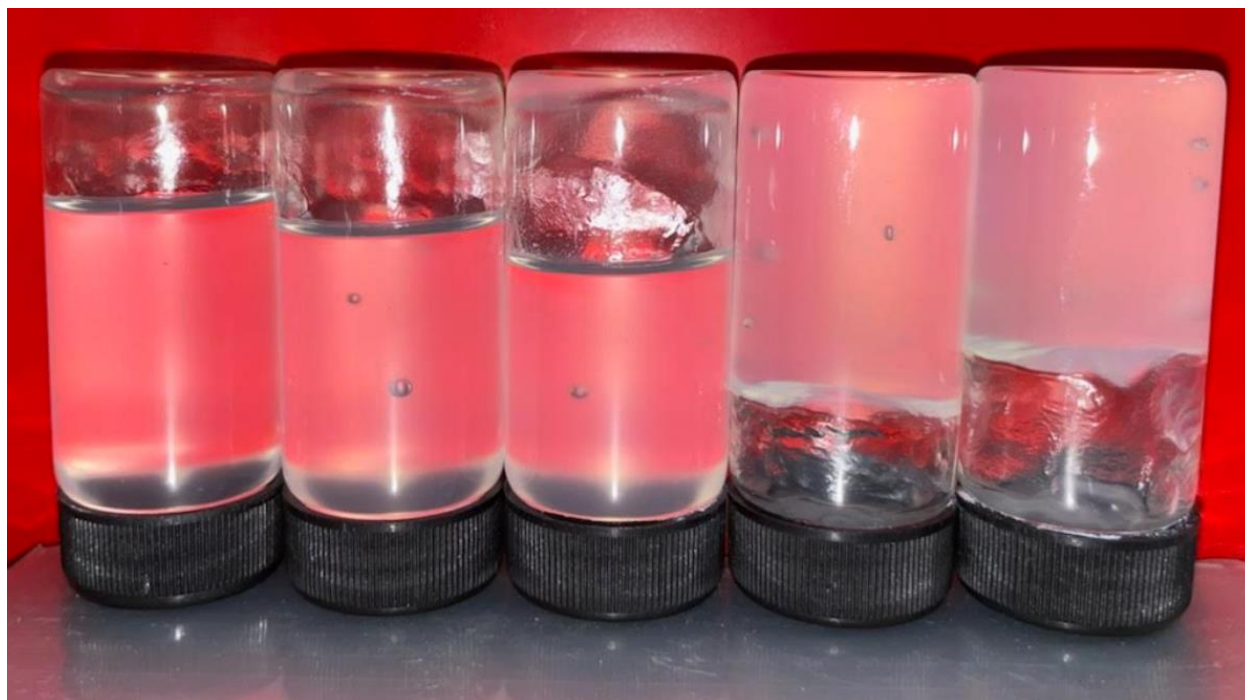


Figure 2.3: Kerosene gelled with a range of 2wt% (left) to 6wt% (right) of fumed silica.

The gel mixtures shown in Figure 2.3 are not the first attempt at formulating a successful gelled fuel. The first gels were formed with the same fumed silica and mixing method but with jet A-1 fuel instead of regular kerosene. These looked promising at first but exhibited poor qualities under shear. When forced through a nozzle, the jet A-1 based gel would largely separate resulting in a thin fluid exiting the nozzle while thick clumps remained clogged inside. This phenomena is the result of the additives in jet A-1 fuel, most likely the additive that prevents clotting when exposed to extremely cold environments. For this reason, standard kerosene was used and the gel could successfully be sheared through the nozzle without separation. It is important to note that successful gelling of jet A-1 fuel has been documented in literature using an organic gelling agent.

Table 2.1: Properties of the gels used in the impact experiments.

Gellant Mass Fraction	Density (g/mL)	Surface Tension (N/m)
0wt%	0.78	30.51
2wt%	0.83	23.24
4wt%	0.92	21.60
6wt%	0.99	21.00

The properties of some of these gels were tested and are displayed in Table 2.1. These gels were used in the subsequent droplet experiments, so these properties are vital for later calculations. The surface tension was measured using the ImageJ pendant drop plugin. This outlines the shape of the droplet to air interface as the fluid exits a nozzle to calculate the surface tension. However, this software will not work for the gels above 4wt% because they do not form pendant drops which can be analyzed. Instead, estimates were made for the thicker gels based on the surface tension trend of the less than 4wt% gels. There is an array of literature discussing the surface tension measurements of highly viscous, non-Newtonian fluids which mainly conclude that estimations are required due to the difficulty of the fluid elasticity and limitations of the measuring equipment.

Additionally, a rheological profile was taken of each gel to form a plot of its viscosity as a function of shear rate. This was done using a TA Instruments DHR-3 rheometer and the plots are included in Figures 2.4-2.8 plotted on a log-log scale. Here, it is clear that each gel is shear thinning and follows the power law equation $\eta = K(\dot{\gamma})^{n-1}$ where η is the dynamic viscosity, $\dot{\gamma}$ is the shear rate, n is the power law coefficient, and K is the consistency coefficient. As expected

the viscosity greatly increases with gellant percentage. As the amount of gellant increases, the n values remain relatively consistent while the K values increase exponentially.

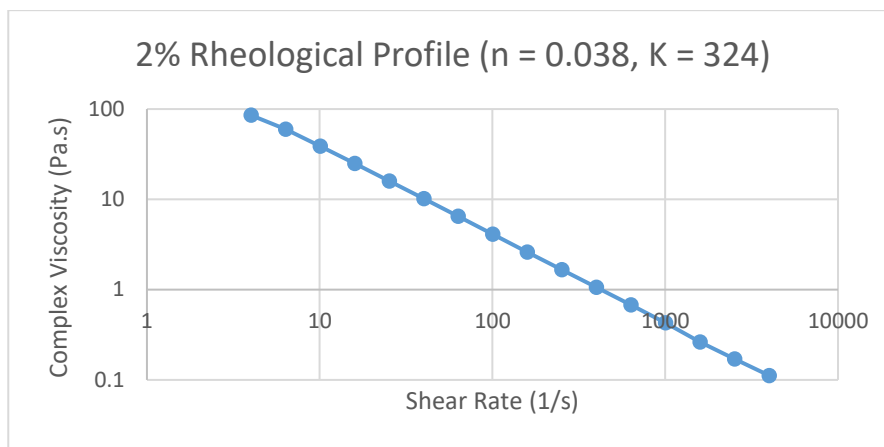


Figure 2.4: Rheological Profile of the 2wt% Gel.

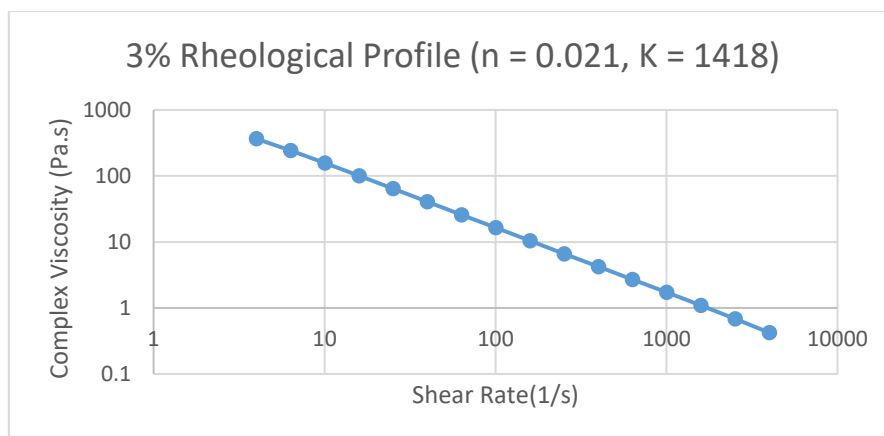


Figure 2.5: Rheological Profile of the 3wt% Gel.

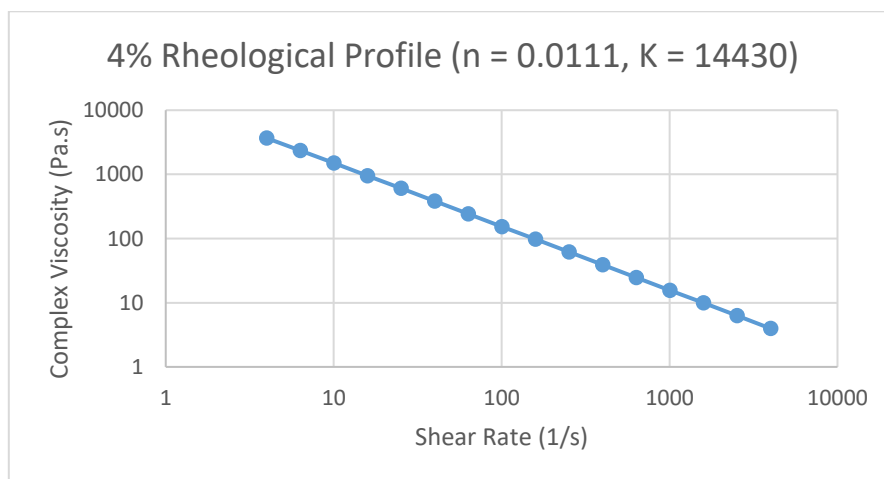


Figure 2.6: Rheological Profile of the 4wt% Gel.

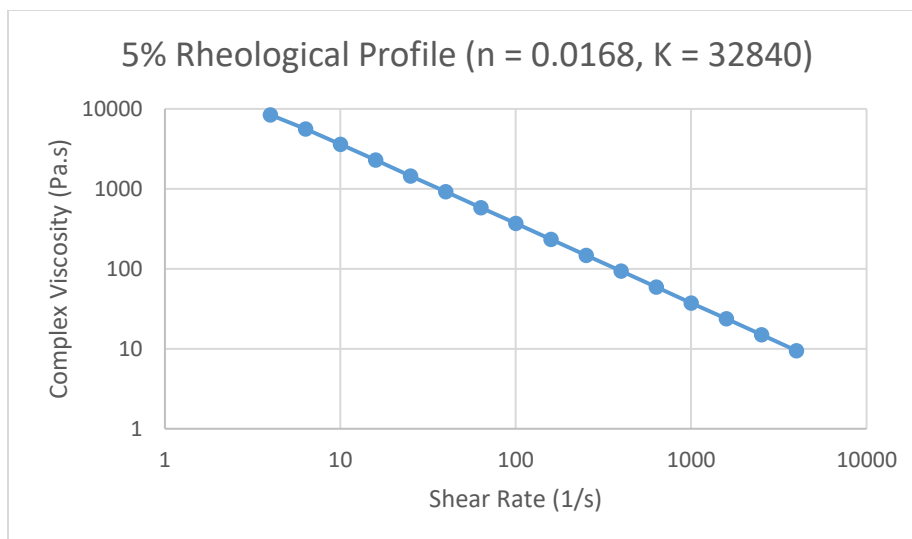


Figure 2.7: Rheological Profile of the 5wt% Gel.

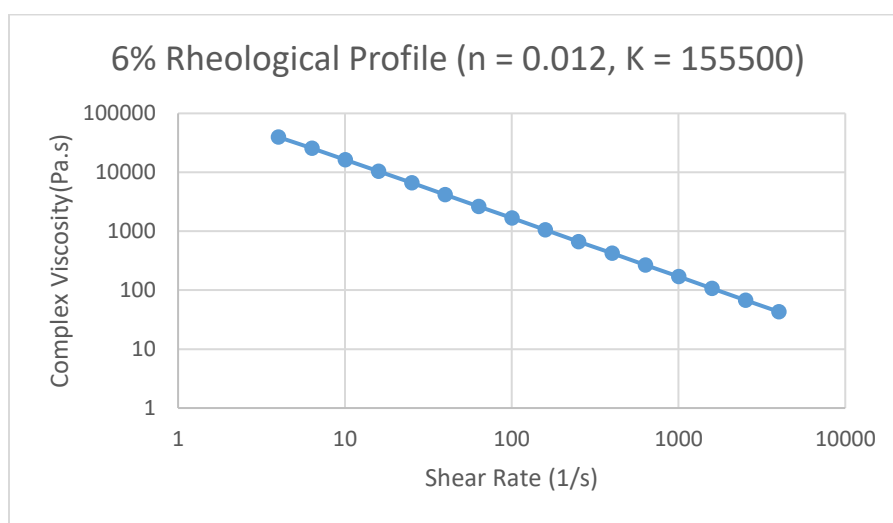


Figure 2.8: Rheological Profile of the 6wt% Gel.

The images used for the surface tension measurements are shown on the left in Figures 2.9 - 2.15. These figures were taken using the high-speed phantom camera mentioned in section 2.1 and binarized using Matlab for better contrast. They show the droplet formation process for each fluid starting with the 0wt% liquid kerosene in Figure 2.9 and progressing to a 6wt% mixture in Figure 2.15. For each fluid, the image on the left shows the maximum droplet size before gravity takes over and the falling process begins. The subsequent three images on the right show the droplet freefall starting at the moment of detachment. The specific times were

chosen to display the oscillatory motion of the fluids and the 1wt% mixture was included to show its similarity to the 0wt% kerosene.

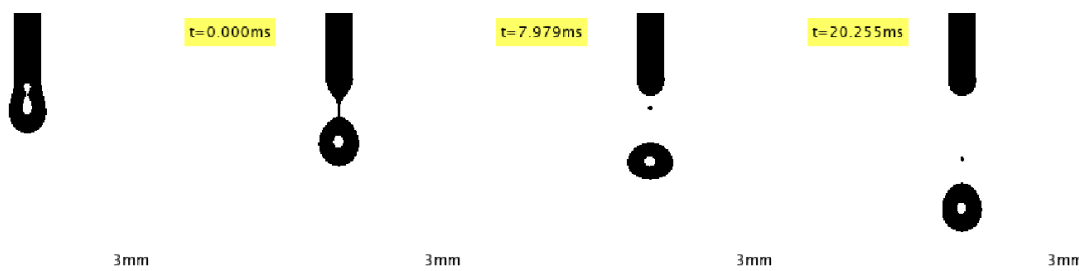


Figure 2.9: 0wt% droplet formation and freefall.

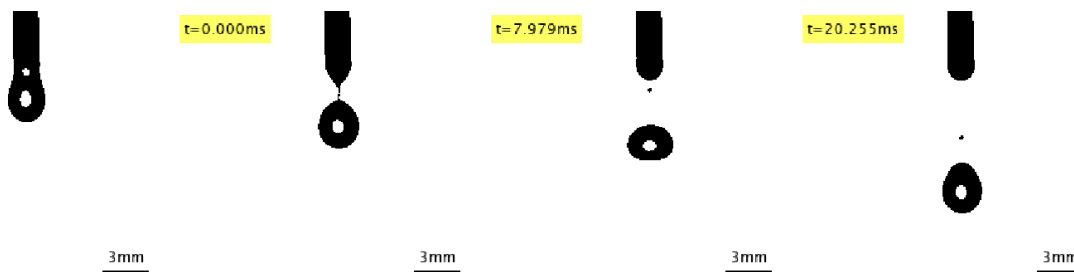


Figure 2.10: 1wt% droplet formation and freefall.

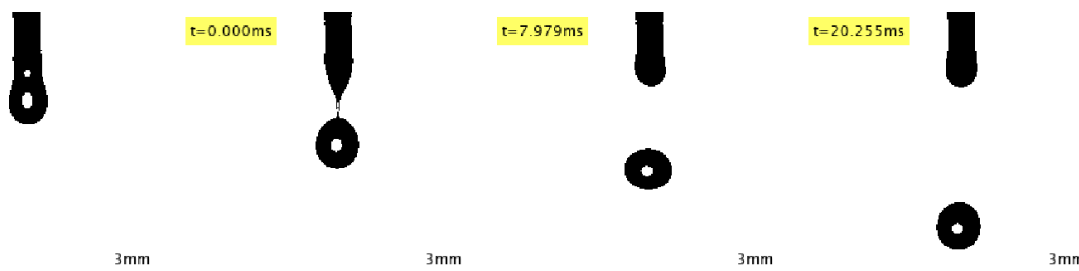


Figure 2.11: 2wt% droplet formation and freefall.

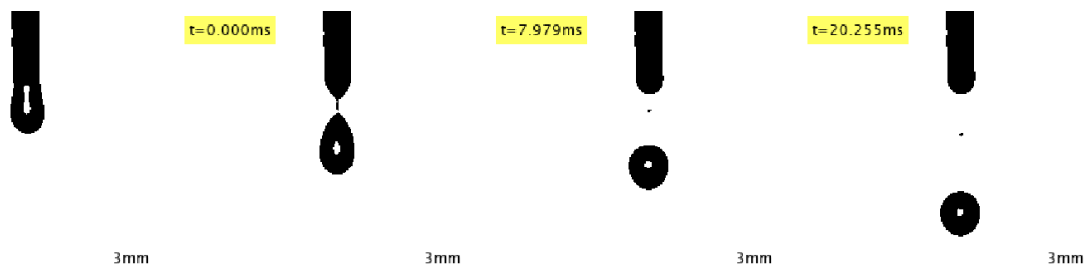


Figure 2.12: 3wt% droplet formation and freefall.

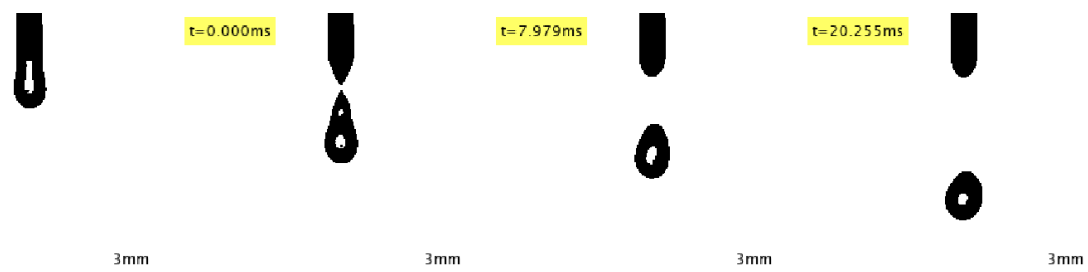


Figure 2.13: 4wt% droplet formation and freefall.

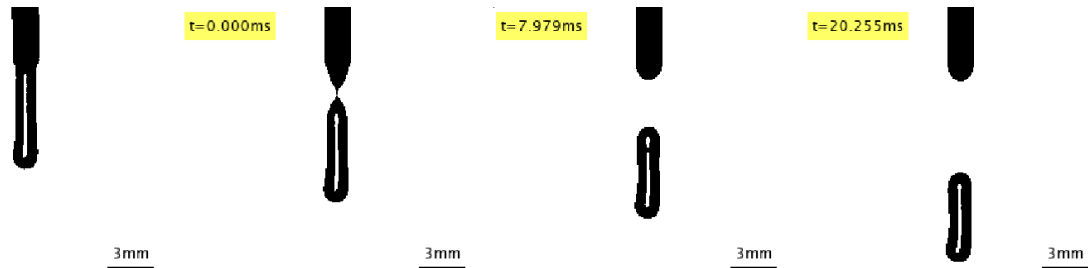


Figure 2.14: 5wt% droplet formation and freefall.

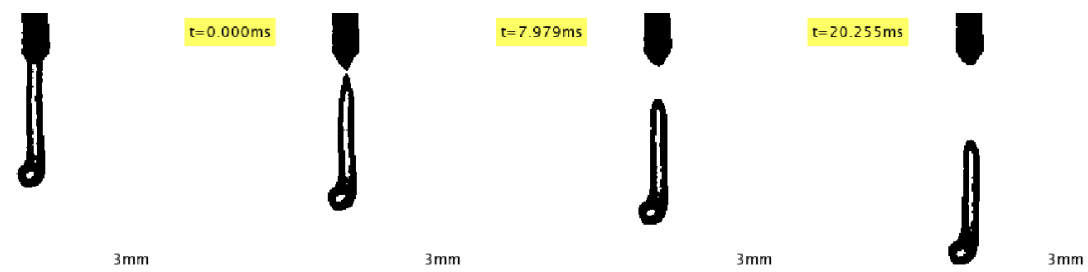


Figure 2.15: 6wt% droplet formation and freefall.

The lower viscosity droplet's oscillatory motion quickly becomes damped as the gellant mass fraction increases. With gellant quantities above 5wt%, the fluid barely changes size over time at all. Table 2.2 shows some of the measurements from the figures like the length of each pendant which indicates elasticity effects as well as the dimensions of the droplets at the moment of their detachment.

Table 2.2: The length of the pendant, height, and width of the droplet for each gel.

Gellant Mass Fraction	Pendant Stretch (mm)	Droplet Height (mm)	Droplet Width (mm)	Height/Width
0wt%	3.4146	3.2520	2.2764	0.7000
1wt%	3.4146	3.2520	2.2764	0.7000
2wt%	3.6585	3.3343	2.9268	0.8778
3wt%	3.7407	4.0650	2.2764	0.5600
4wt%	3.7407	5.0406	2.2764	0.4516
5wt%	7.3171	7.0732	1.7073	0.2414
6wt%	9.5935	9.3496	1.2195	0.1304

Once the gelling percentage reaches 5wt%, elastic effects take over greatly increasing the size of each droplet as well as influencing its shape. This effect is somewhat present in the slightly deformed 4wt% droplet but is not near the same degree as the 5wt% and 6wt% gels which are strongly deformed. This leads to difficulties in determining the exact volume of the thicker gels. The volume for each droplet of the gels of 4wt% and less can be directly measured due to their spherical shape. To determine the size of the 6wt% droplets, the average mass of ten droplets was taken. This, with the density measurements, gives the average volume of the 6wt%

droplet which is 20.84 millimeters cubed. This value is used as an approximation for the 6wt% droplet volume when performing calculations around the droplet impact experiments.

2.3 Weber Number Calculations

An important dimensionless value in predicting the outcome of the behavior of fluid-on-fluid interfaces is the Weber number (We). This is especially useful when concerning the breakup and formation characteristics of droplets as well as their dynamics. It is expressed as a ratio of the resistant drag forces on the droplet to its surface tension holding it together. It can be calculated using the equation below where ρ is the density, v is the velocity, σ is the surface tension, and L is the characteristic length or the droplet diameter in this case.

$$We = \frac{\rho v^2 L}{\sigma}$$

Droplets can reach velocities at which the drag forces overcome the surface tension force in the droplet resulting in breakup. Regarding velocity measurements, the measured velocity was consistently smaller than that predicted by the equations of motion suggesting that air resistance is not negligible in this case. Therefore, the weber number will not scale directly with height as would be the case without air resistance. The Weber number calculation in this paper are accurate so long as the droplets can form spheres. As observed, the thicker 6wt% gel does not form into a spherical shape at all but instead a long cylinder. Therefore, the characteristic length must be approximated based on the angle of the falling cylinder. This approximation, combined with the estimates for the surface tension, makes the Weber number calculations for the 6wt% gel much more inaccurate than the same calculations for the other gels. However, this is the only gel in which the Weber number calculations rely on approximations as the other gels form spheres so the diameter and surface tension can be measured.

CHAPTER 3

RESULTS AND DISCUSSION

3.1 Effect of Gellant Percentage

Three variables are being altered in these test, the droplet height, the surface material, and the mixture gellant percentage of which the strongest changes come from altering the gellant concentration. This can be seen when analyzing the results of the impacts onto a smooth glass surface from 50cm. Figures 3.1-3.4 show timelines of the impact of a droplet of each gel onto the glass surface. These were taken in a similar way to the droplet formation pictures and binarized using Matlab. The timescale is set so that time is zero at the last frame before the droplet comes into contact with the surface.

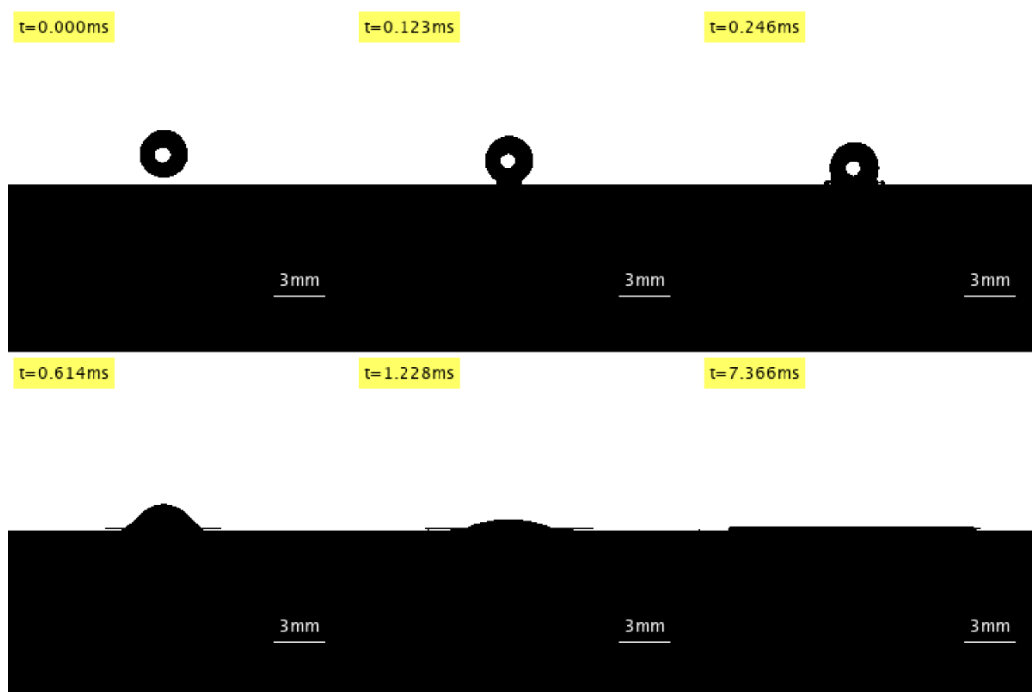


Figure 3.1: 0wt% impact onto smooth glass from 50cm.

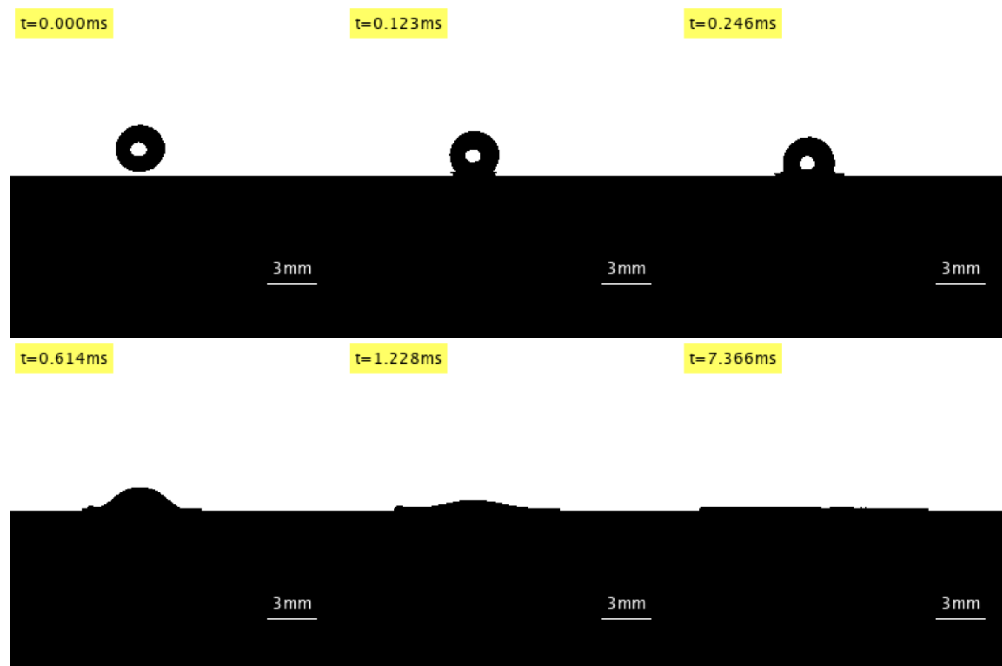


Figure 3.2: 2wt% impact onto smooth glass from 50cm.

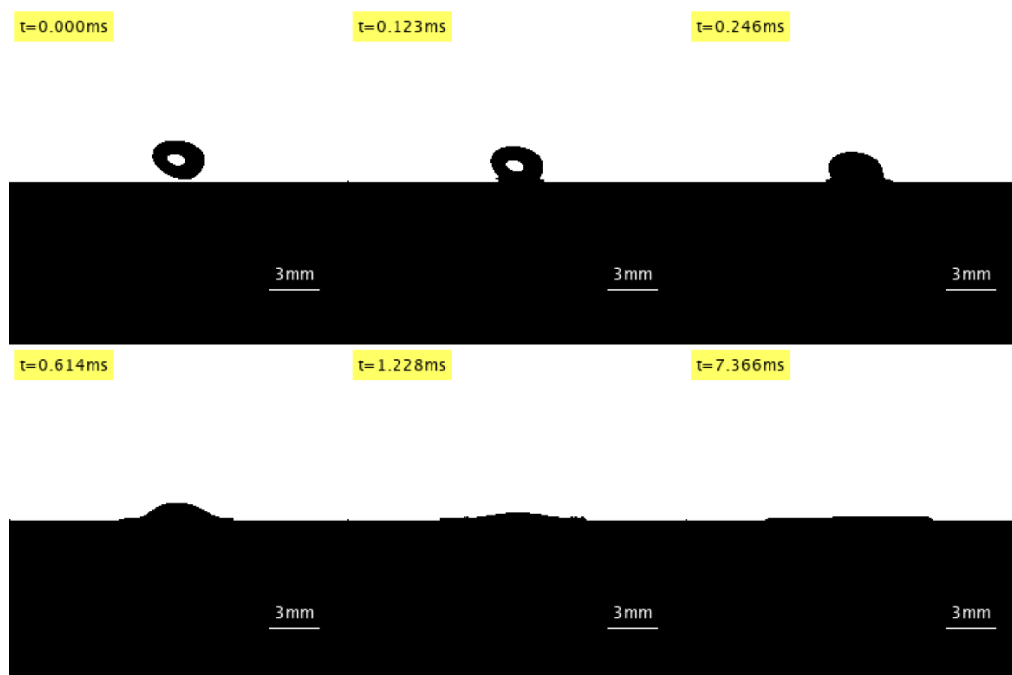


Figure 3.3: 4wt% impact onto smooth glass from 50cm.

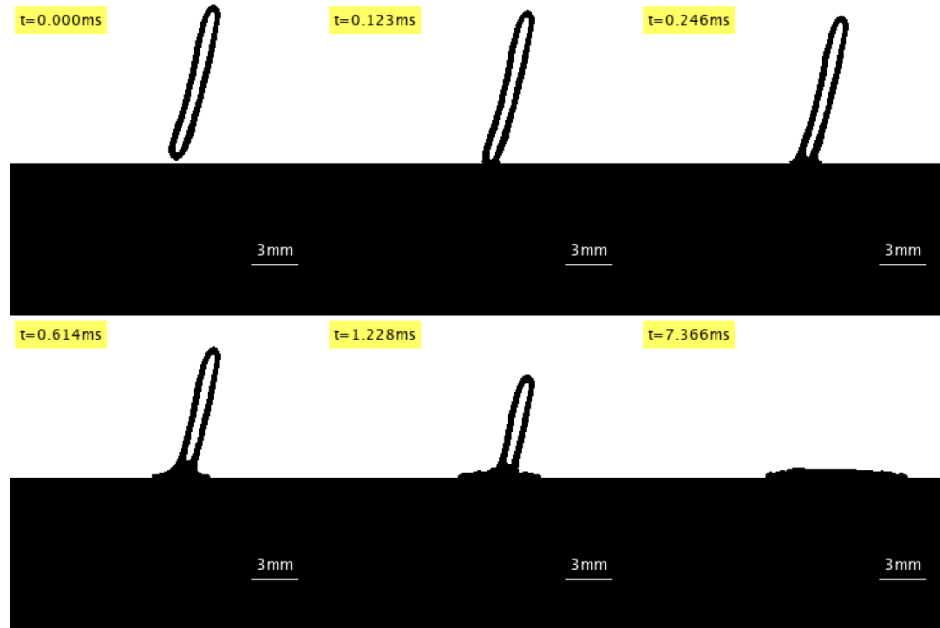


Figure 3.4: 6wt% impact onto smooth glass from 50cm.

Based off these images, the impacts have some similarities and differences. Namely, there is no rebounding effect. Each fluid impacts the surface, spreads until it reaches a certain diameter and stops with no regression thereafter except for that being caused by evaporation. This kind of impact is known as sticking. It is also clear that the higher gellant percentage droplets spread over a smaller surface area while maintaining a thicker layer over the surface. To get a better understanding of the spread characteristics, Figure 3.5 shows the images from above using the DSLR camera of each fluid, 0wt%, 2wt%, 4wt%, and 6wt% from left to right. Both the top and bottom images have been put into grayscale and the bottom images have also been binarized. From these images, the decrease in spread area does not appear to have a linear relationship with gellant percentage as the 2wt% gel has a larger spread area than the pure kerosene.

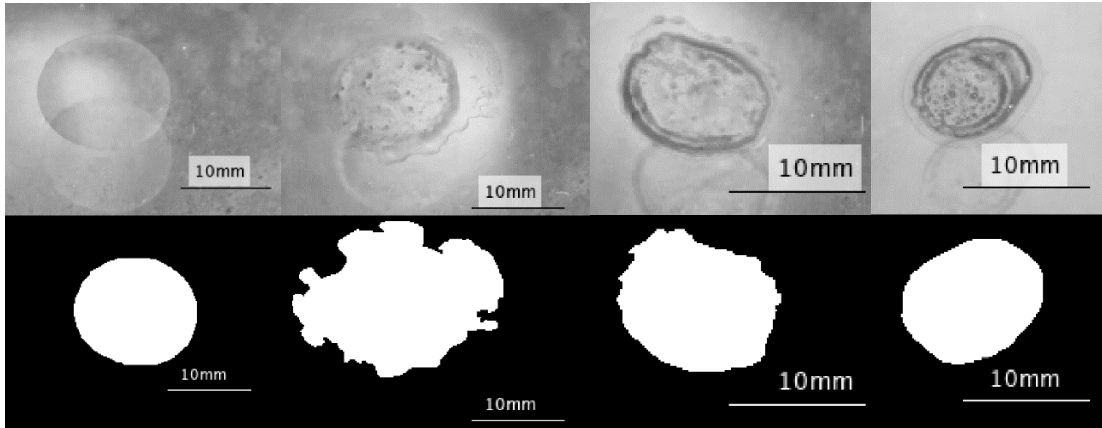


Figure 3.5: Spread comparison from 50cm onto smooth glass for 0wt% (left) to 6wt% (right).

The spread area was calculated using the ImageJ measurement tool. It is important to note the 28° angle of the DSLR camera influences the pixel aspect ratio. That is the ratio of the width of each pixel to its height. For the given camera angle, the pixel aspect ratio is 1.133 allowing for area calculations. These calculations are included in Table 3.1 along with other important impact characteristics. Of these is the Reynolds number at the moment of impact which determined using the following equation for Newtonian fluid flow:

$$Re = \frac{\rho v L}{\eta}$$

However, for power law fluids the viscosity is not known. Therefore, for all my gels the generalized Reynolds number is used. This is documented in research such as that by Luu and Forterre (2009) and is given by the following equation where n is the power law coefficient and K is the consistency coefficient which are determined based on the rheological data for each gel.

$$Re_n = \frac{\rho v^{2-n} L^n}{K}$$

An important talking point here is the presence of an inner and outer spread diameter for the 2wt% and 4wt% gels. This is present throughout almost all the tests and the spread area will be calculated based off the larger spread diameter. This additional spread area occurs on a scale

of seconds instead of milliseconds as it is not captured by the high-speed camera. Although not fully understood, the outer spread is likely a result of impact shock partly breaking apart the gel structure resulting in separation. This phenomenon is much more pronounced for the lower wt% gels and tapers off becoming essentially nonexistent for many of the 6wt% impacts.

Table 3.1: Impact characteristics from 50cm onto smooth glass.

Gellant Percentage	Volume (mm³)	Weber Number	Spread Diameter (mm)	Spread Area (mm²)	Reynolds Number
0wt%	12.59	0.80	15.20	61.14	3.464
2wt%	14.84	1.03	14.23	101.32	18.43
4wt%	11.55	1.08	10.41	37.49	0.5017
6wt%	20.84	1.14	9.35	33.30	0.04996

These calculations confirm that the 2wt% gel increases the surface area by a large amount while the 4wt% and 6wt% gels decrease the spread area. This is even more interesting when considering the larger volume of the 6wt% gel. Even though it has almost twice the volume of the pure kerosene droplet, it still decreases the spread area by almost half. It is also interesting that the 4wt% has positive effect on the spread area while still being able to form a rough sphere while in freefall and flow of its own accord.

3.2 Changing Weber number

With the gelled fuel reducing the spread area well at 50cm, tests were also performed to see if the results are consistent at 100cm. Similar images as the ones in the previous section displaying the droplet impact over time are shown in Figures 3.6-3.9 and splash profiles for each gel impact are shown in Figure 3.10.

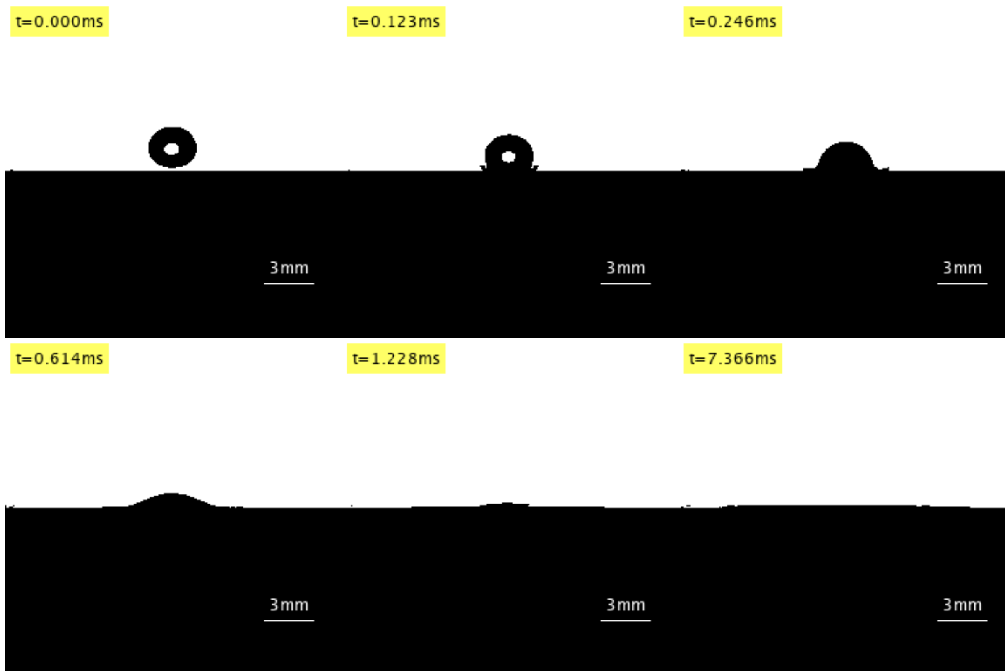


Figure 3.6: 0wt% impact onto smooth glass from 100cm

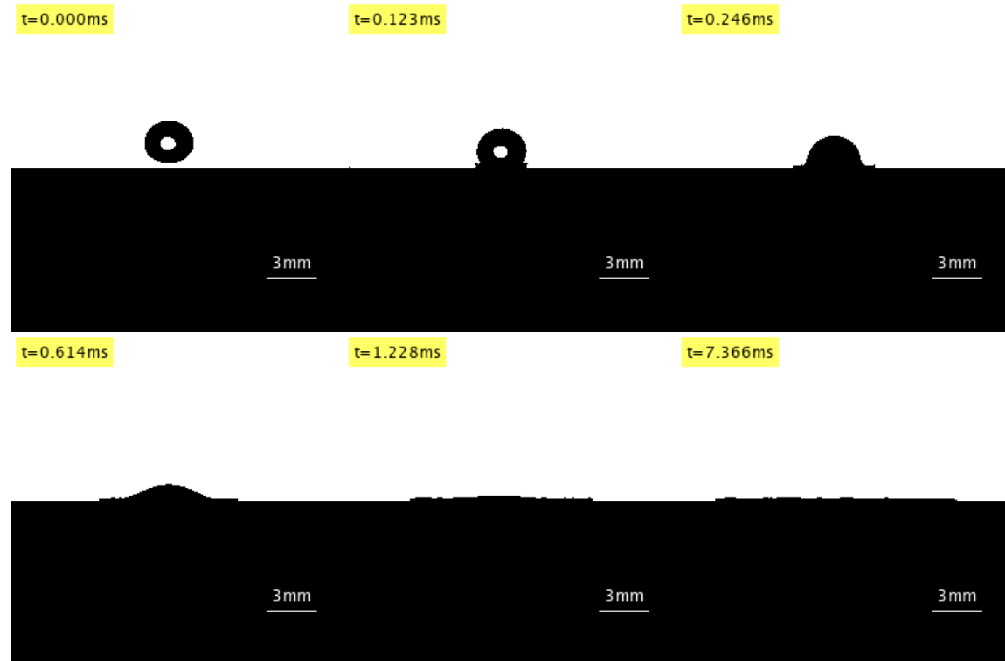


Figure 3.7: 2wt% impact onto smooth glass from 100cm

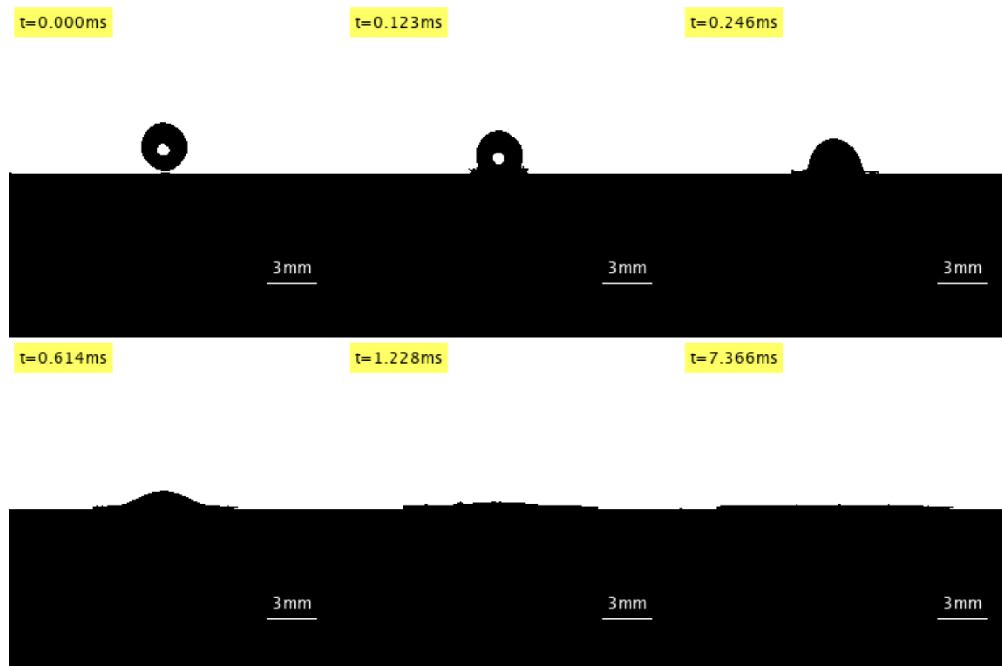


Figure 3.8: 4wt% impact onto smooth glass from 100cm

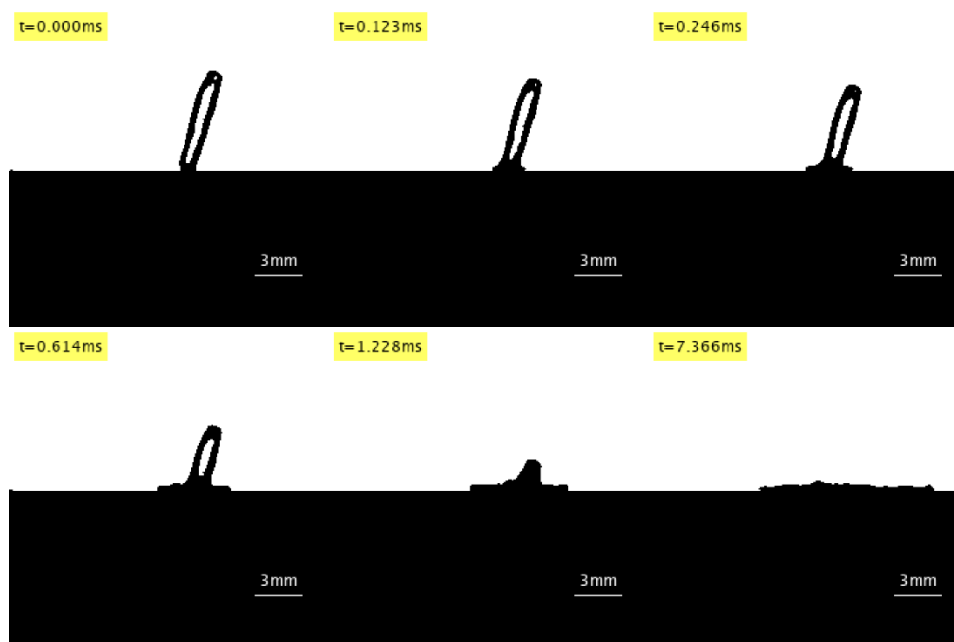


Figure 3.9: 6wt% impact onto smooth glass from 100cm

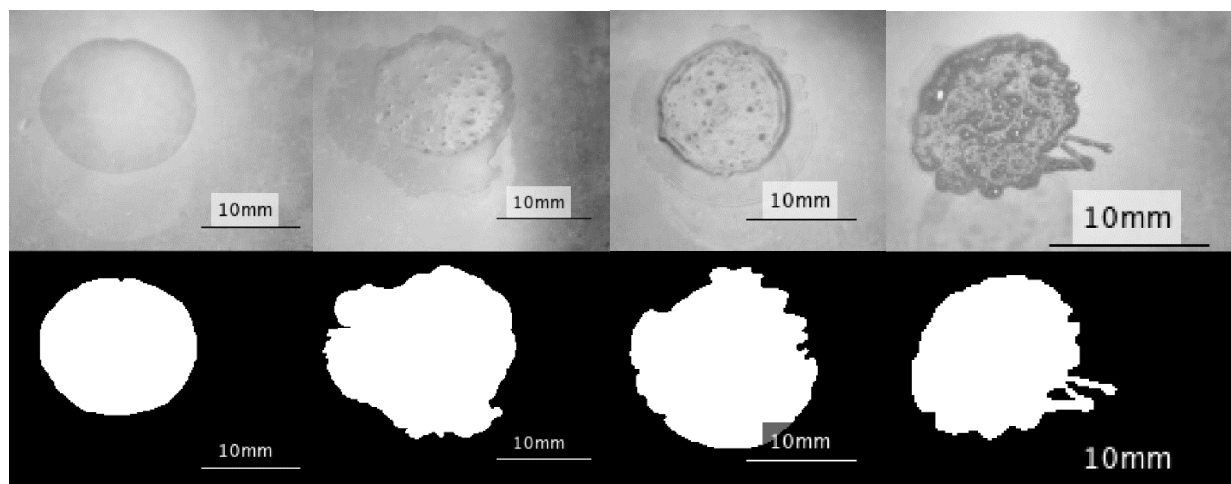


Figure 3.10: Spread comparison from 50cm onto smooth glass for 0wt% (left) to 6wt% (right).

Table 3.2: Impact characteristics from 100cm onto smooth glass.

Gellant Percentage	Volume (mm³)	Weber Number	Spread Diameter (mm)	Spread Area (mm²)	Reynolds Number
0wt%	11.06	1.10	15.45	71.04	4.862
2wt%	12.06	1.30	15.12	110.67	30.89
4wt%	13.68	1.47	14.72	81.19	0.9947
6wt%	20.84	1.36	11.46	34.31	0.08056

Again, the results are displayed in Table 3.2 for analysis. The weber number increases by around 0.30 for each gel when increasing the height from 50cm to 100cm with the exception of the 6wt% gel. The difficulty of calculating the weber number for the thicker gels was discussed in section 2.3 so this anomaly is within the bounds of error for an estimation of the Weber number. The increase in Weber numbers leads to a larger spread area for each gel when compared to the slower impact. The area of the 0wt% and 2wt% fluids increased by roughly 10 mm² while the 4wt% increased by over 40mm² and the 6wt% spread area hardly increased at

all. The results are like those in section 3.2 other than the spread area for the 4wt% gel being larger than the spread area of the 0wt% gel. This is not entirely consistent with the data taken in the next sections as will be discussed. It is important to note that the spread area of the kerosene film for this 4wt% droplet impact was much larger than the standard 4wt% impact. This could indicate additional separation occurring during the impact shock or might be a result of the unpredictable nature of the outer spread area. The viscous 6wt% gel still showed excellent improvements in spread area decreasing this value by more than a factor of two over the 0wt% gel.

To better compare the spread effects from all the impacts, I plotted the spread diameter change over time starting at the moment of impact. This is shown in Figure 3.11 with a general trend of the higher percentage of gellant and a lower height producing the least amount of spread. Additionally, the largest spread rate occurs in the frames just after impact and decreases until the spread reaches a stable diameter. An important note here is that these were measured using the high-speed camera and thus do not capture the longer scale settling of the kerosene gel. Therefore, the spread diameter in these plots will not include the thin outer ring which takes many seconds to fully form but only the thick inner ring which reaches a stable formation within the first second of impact. Regarding this inner spread area, it shows very consistent trends of decreasing with an increase in gellant percentage for each impact. This is the assumed spread area if the outer spread can be eliminated. With this in mind, the data for the inner spread diameter shows promising results for the safety of these gels.

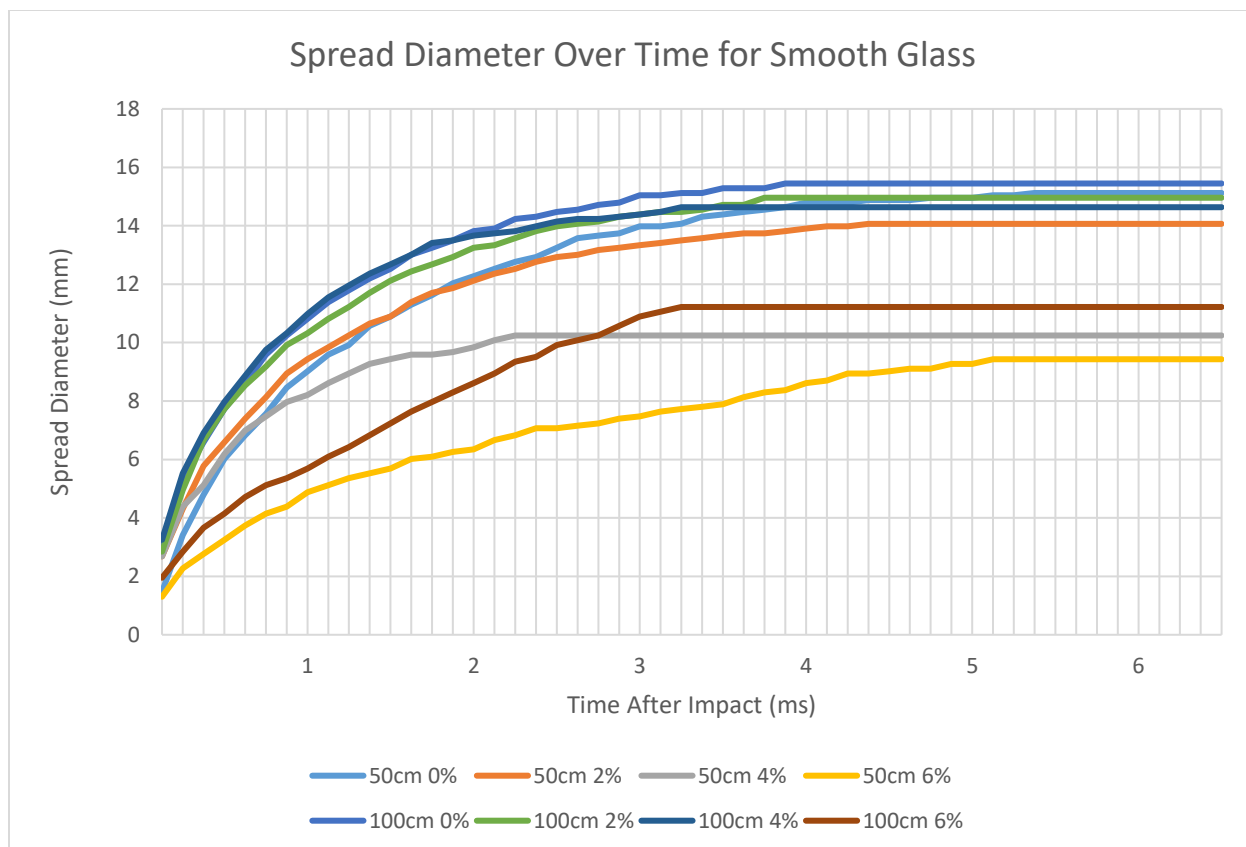


Figure 3.11: The spread diameter over time for each impact onto the smooth glass.

3.3 Different surface effects

Now, glass is not the most likely substance for kerosene impacts. So similar impact experiments are performed on four more different materials, aluminum, nickel, stainless steel, and smooth oleophobic glass.

3.3.1 Aluminum

Starting with aluminum, Figures 3.12-3.19 show the impact for each gel onto an aluminum plate from both 50cm and 100cm. Similarly, Figures 3.20 and 3.21 show the spread characteristics of each impact while Tables 3.3 and 3.4 outline the key impact parameters.

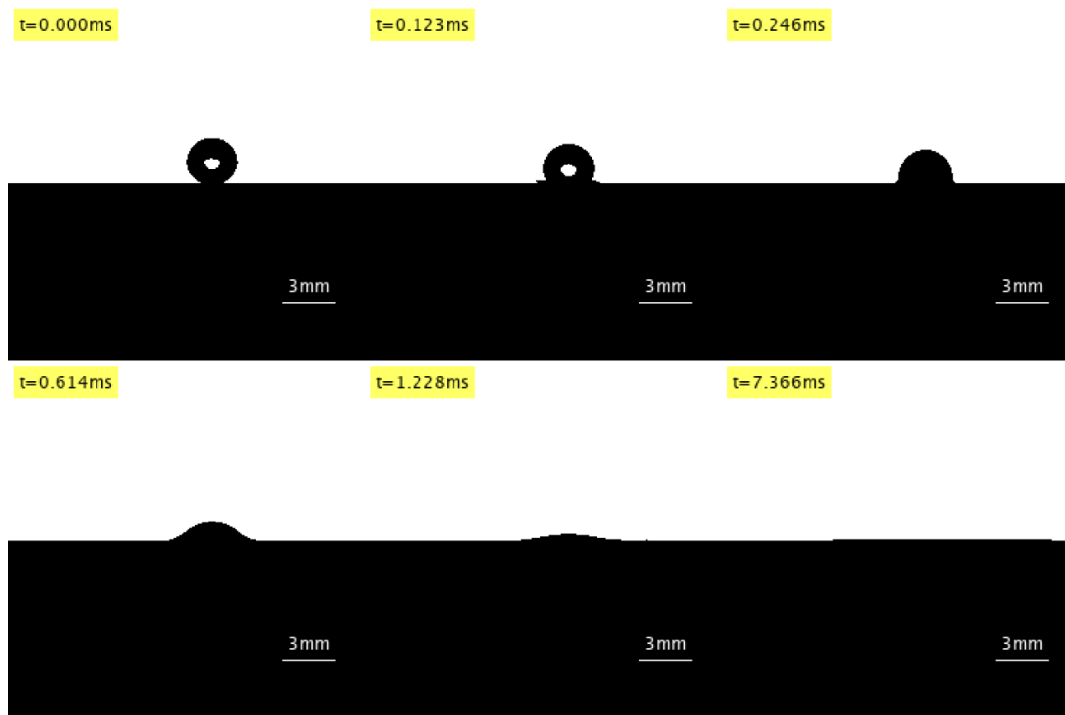


Figure 3.12: 0wt% impact onto aluminum from 50cm.

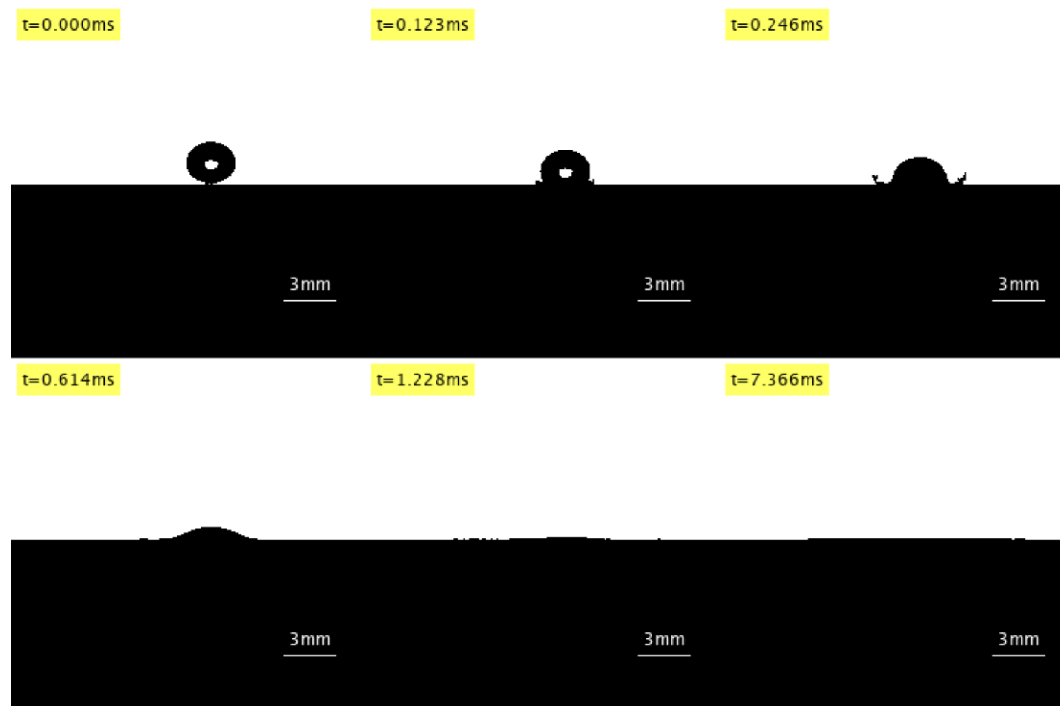


Figure 3.13: 0wt% impact onto aluminum from 100cm.

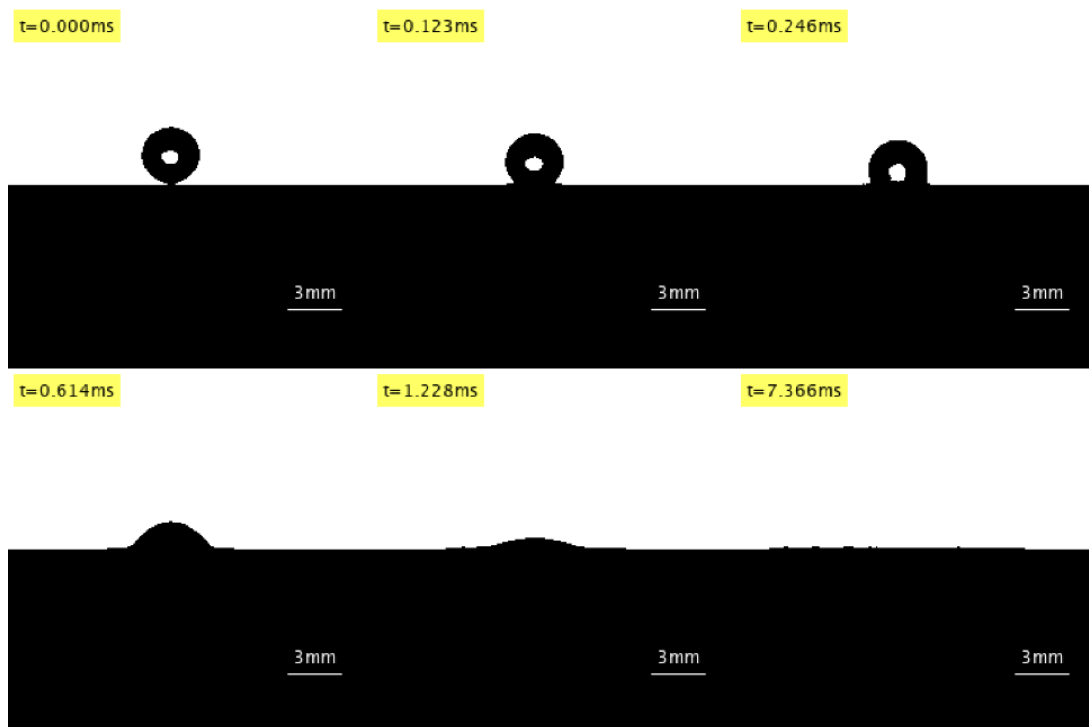


Figure 3.14: 2wt% impact onto aluminum from 50cm.

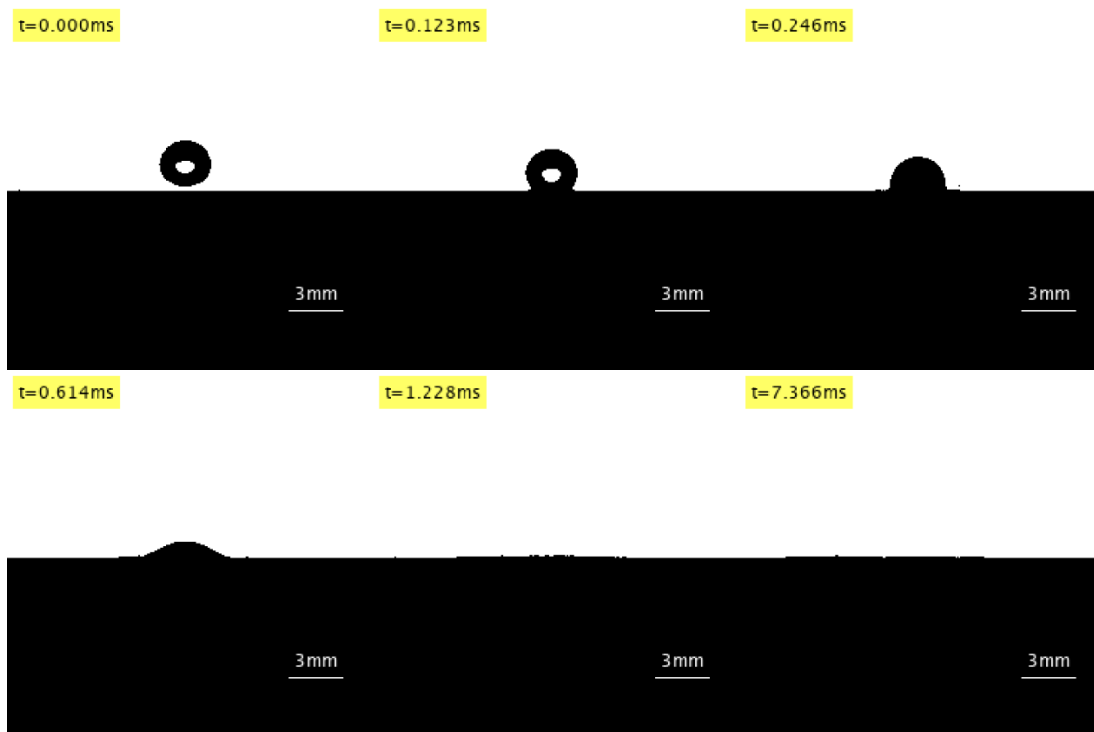


Figure 3.15: 2wt% impact onto aluminum from 100cm.

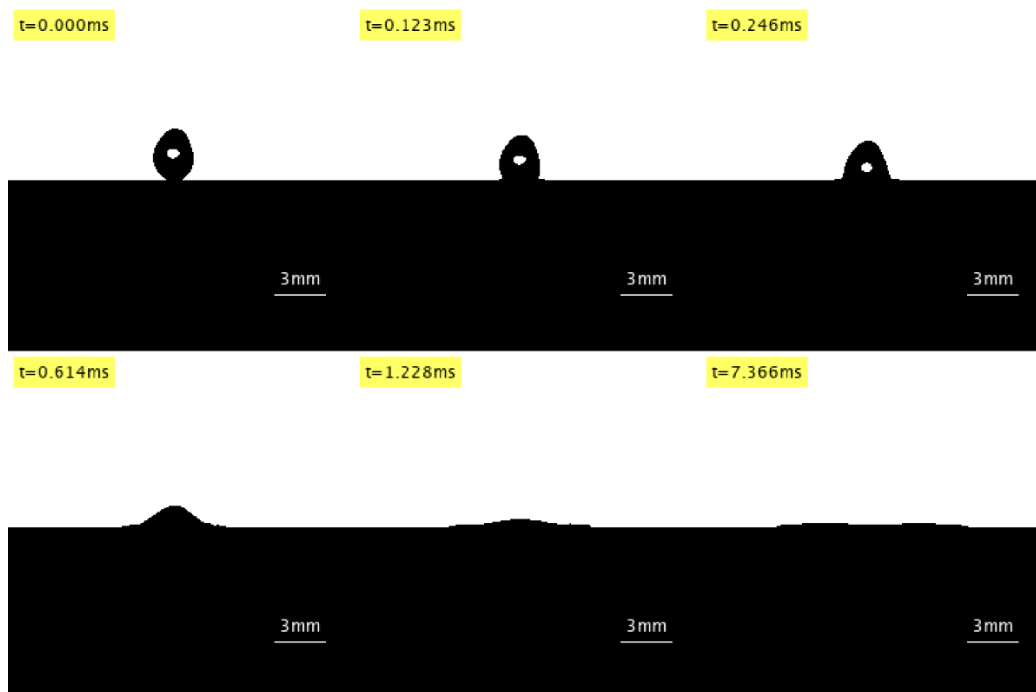


Figure 3.16: 4wt% impact onto aluminum from 50cm.

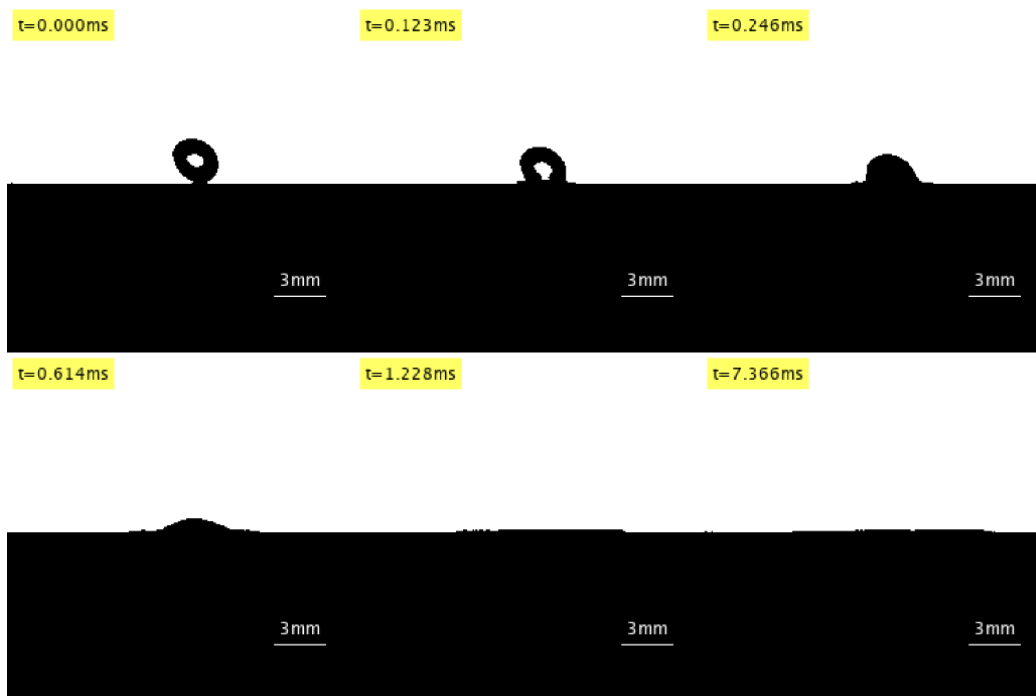


Figure 3.17: 4wt% impact onto aluminum from 100cm.

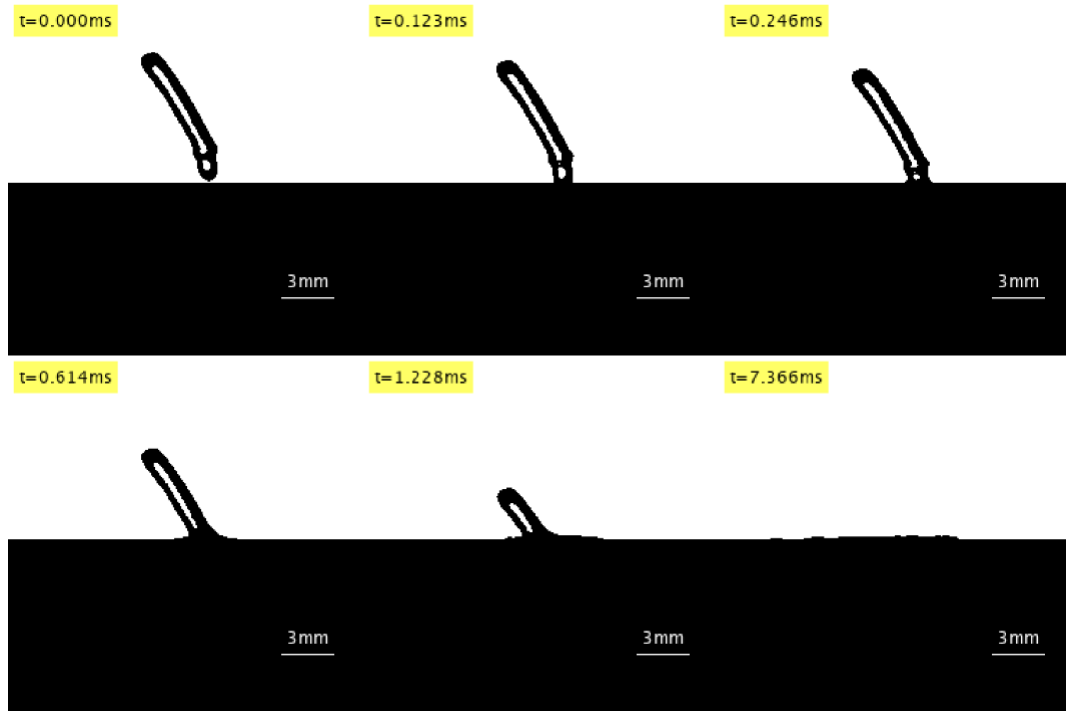


Figure 3.18: 6wt% impact onto aluminum from 50cm.

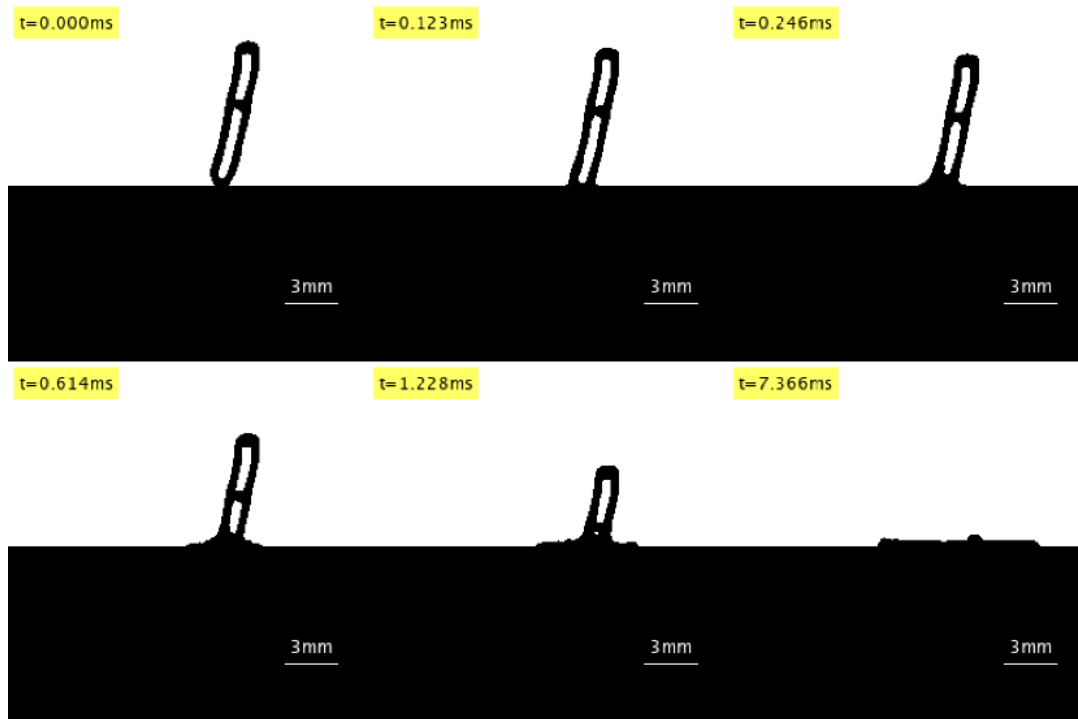


Figure 3.19: 6wt% impact onto aluminum from 100cm.

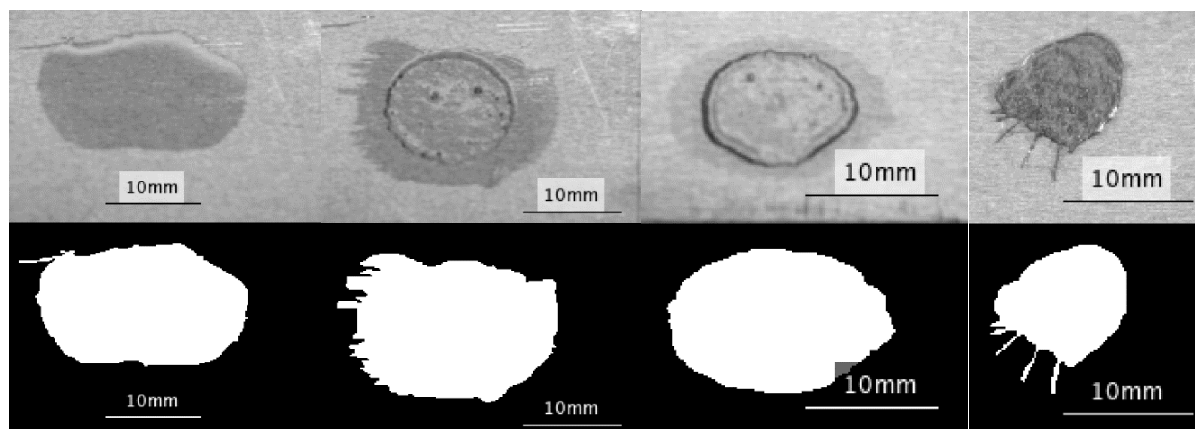


Figure 3.20: Spread comparison from 50cm onto aluminum for 0wt% (left) to 6wt% (right).

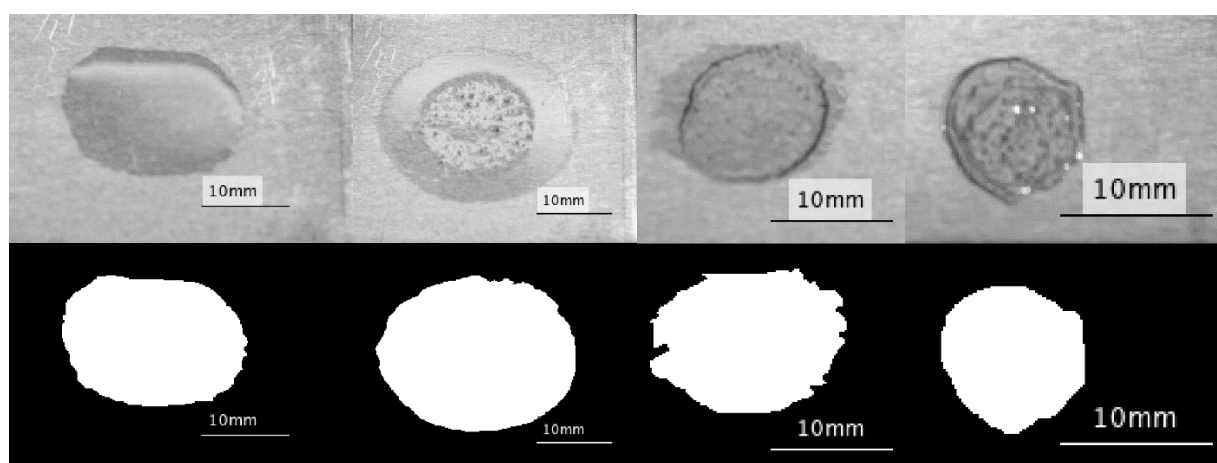


Figure 3.21: Spread comparison from 100cm onto aluminum for 0wt% (left) to 6wt% (right).

Table 3.3: Impact characteristics from 50cm onto aluminum.

Gellant Percentage	Volume (mm³)	Weber Number	Spread Diameter (mm)	Spread Area (mm²)	Reynolds Number
0wt%	11.06	0.80	14.96	94.61	3.464
2wt%	14.84	1.05	14.80	102.09	18.38
4wt%	11.55	0.94	11.38	57.26	0.5001
6wt%	20.84	0.99	9.35	28.32	0.04962

Table 3.4: Impact characteristics from 100cm onto aluminum.

Gellant Percentage	Volume (mm³)	Weber Number	Spread Diameter (mm)	Spread Area (mm²)	Reynolds Number
0wt%	9.66	1.23	14.96	103.25	5.353
2wt%	11.55	1.26	14.96	170.90	28.90
4wt%	12.07	1.36	11.71	58.44	0.8681
6wt%	20.84	1.72	9.19	27.34	0.08101

Clearly the addition of gelling agent beyond a certain point, around 4wt%, dramatically improves the spread area for impacts onto aluminum. The 2wt% gel still causes an increase in spread area over the 0wt% and the 4wt% gel is now also showing an improvement in spread area. We can also confirm that the increase in Weber number of the 100cm drops has a negligible effect on the spread area of the 4wt% and 6wt% gels. Higher, faster drops would be necessary to achieve a larger Weber number to determine more accurate relationships between the Weber number and spread area for each gel. The spread diameter remains consistent with the previous data trending downward with an increase in gelling percentage. Again, a plot comparing the spread diameters as a function of time is included in Figure 3.22.

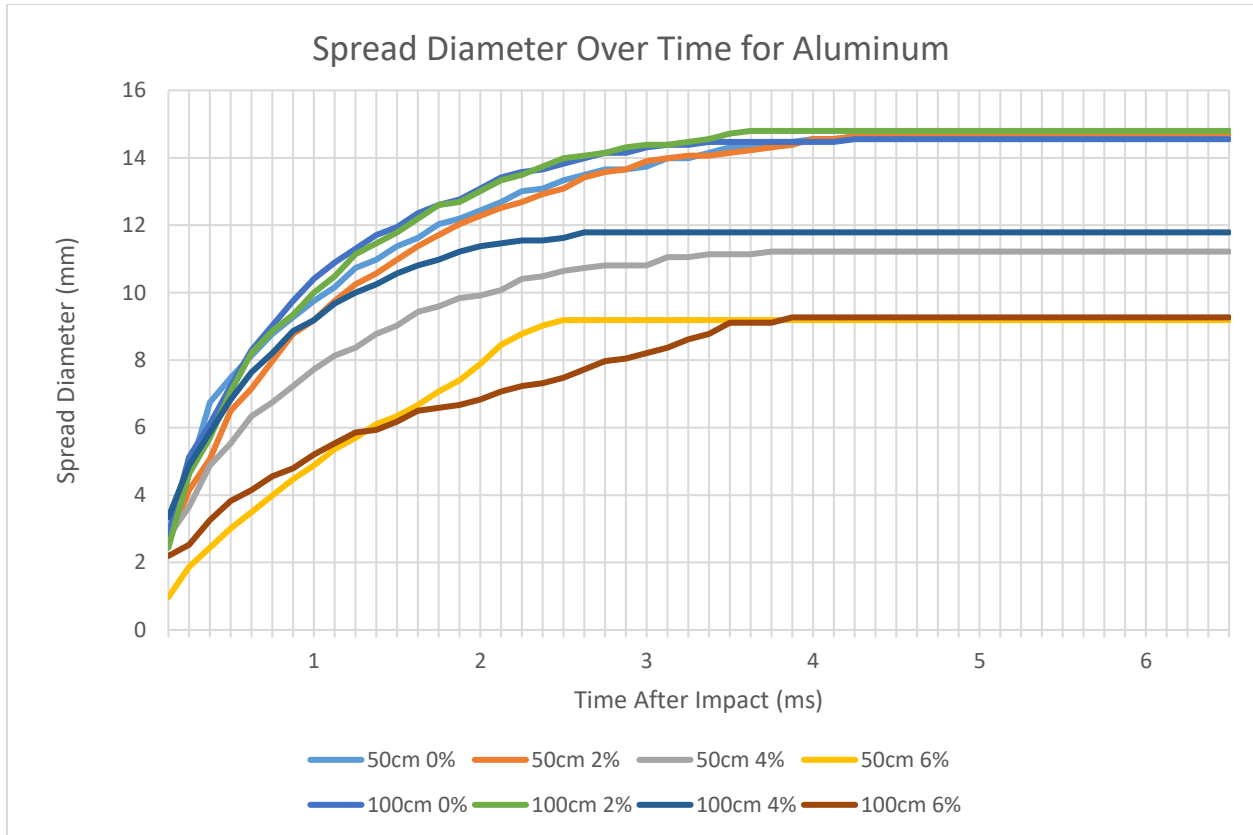


Figure 3.22: The spread diameter over time for each impact onto the aluminum surface.

3.3.2 Nickel

The results for the nickel impact experiments are displayed similarly to the previous sections with Figures 3.23-3.30 showing the impacts of each gel from both heights onto the nickel alloy, Figures 3.31 and 3.32 showing the splash area from above, and Tables 3.5 and 3.6 displaying the key impact characteristics.

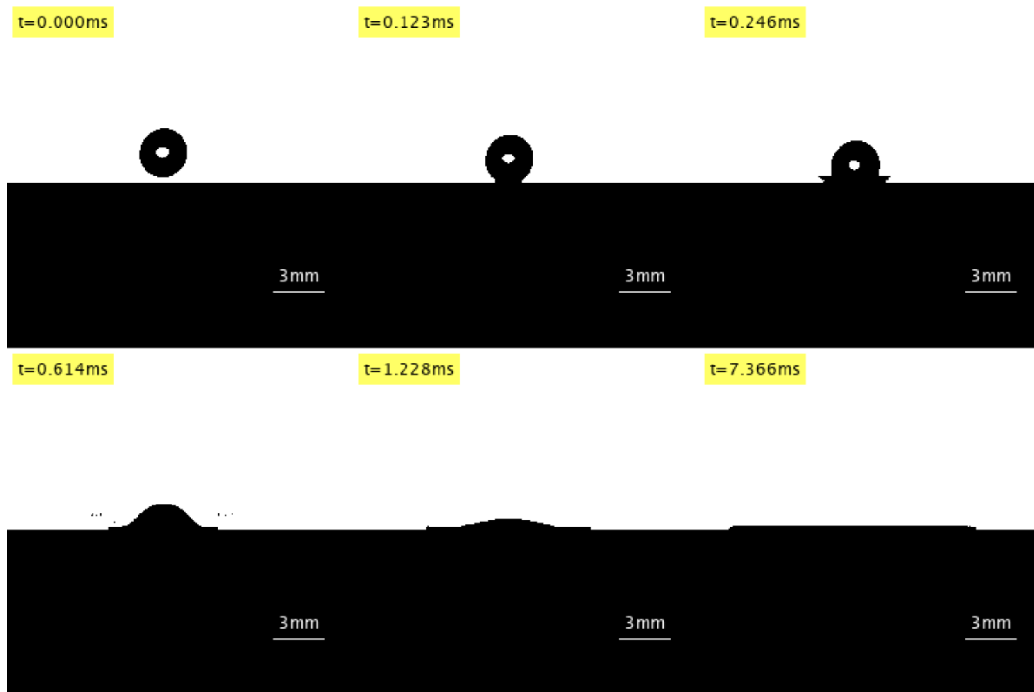


Figure 3.23: 0wt% impact onto nickel from 50cm.

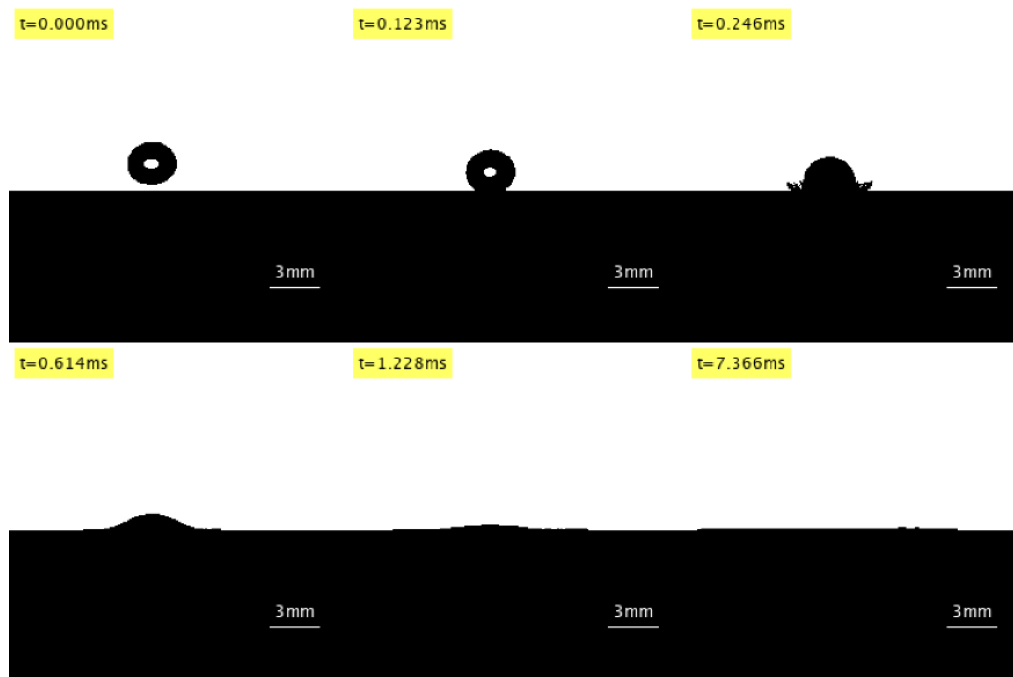


Figure 3.24: 0wt% impact onto nickel from 100cm.

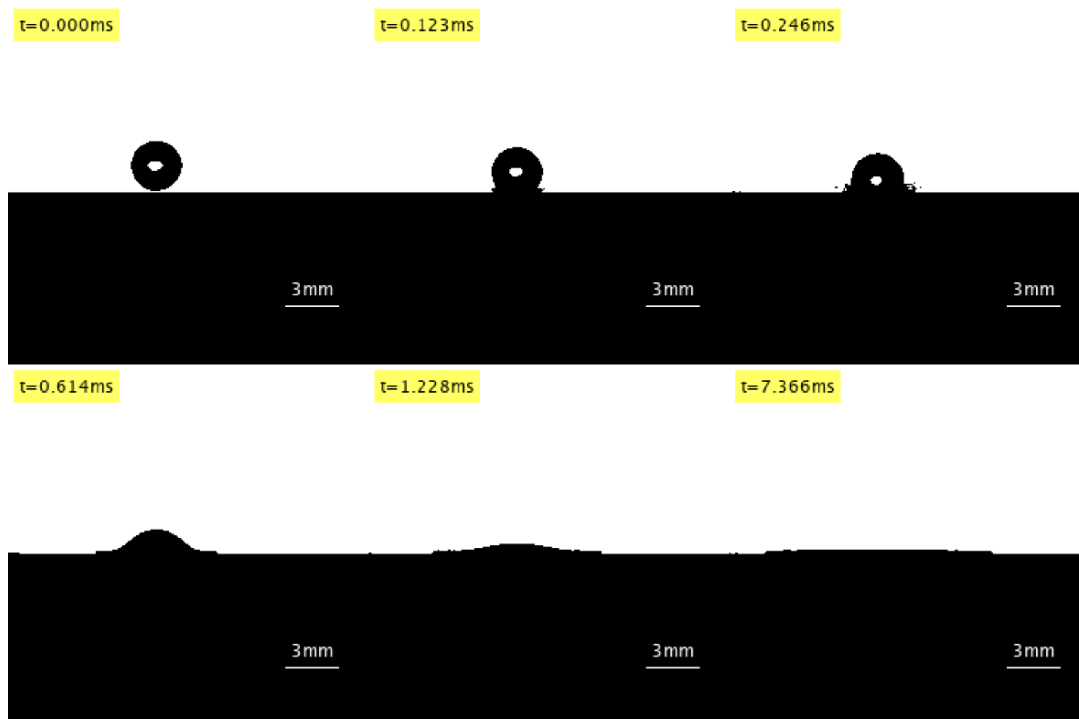


Figure 3.25: 2wt% impact onto nickel from 50cm.

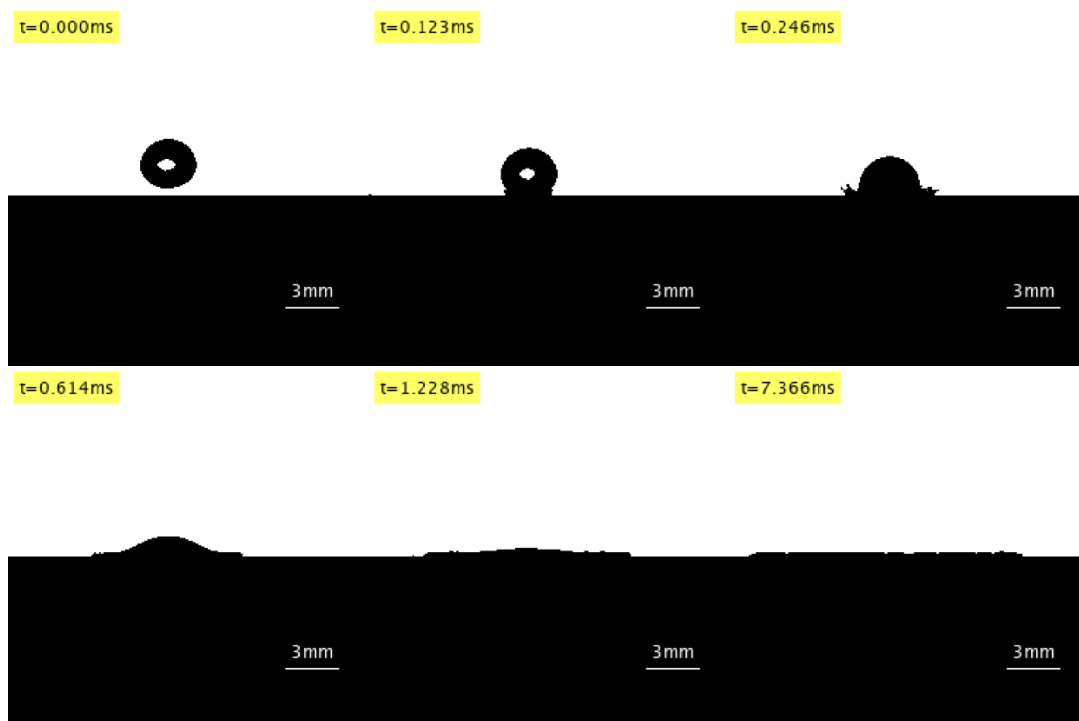


Figure 3.26: 2wt% impact onto nickel from 100cm.

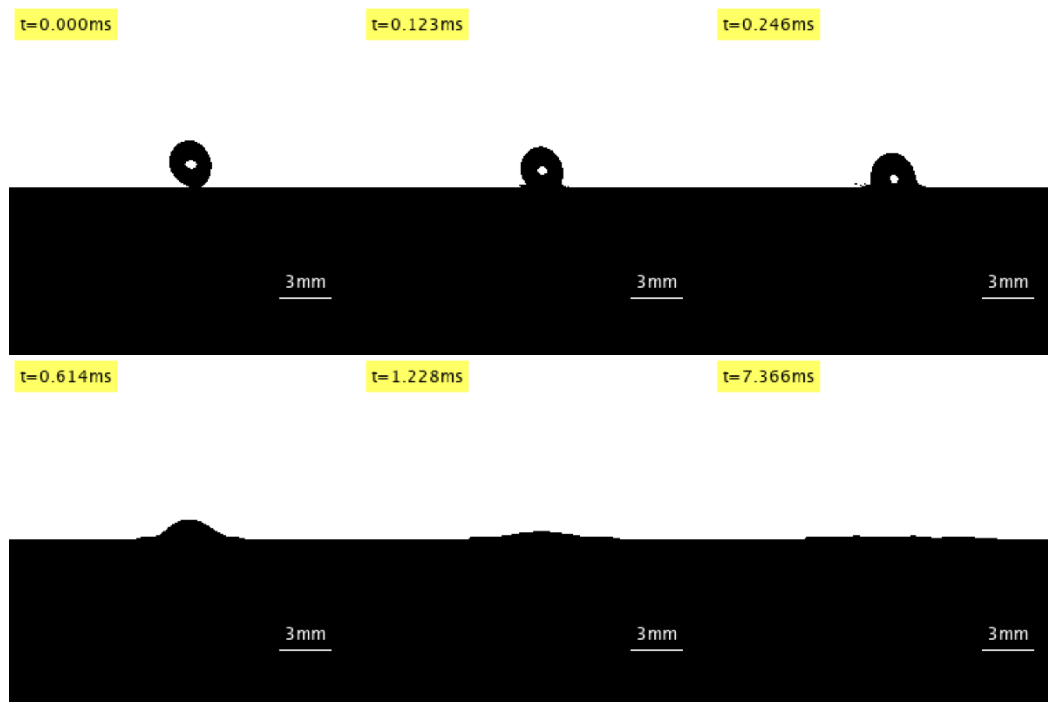


Figure 3.27: 4wt% impact onto nickel from 50cm.

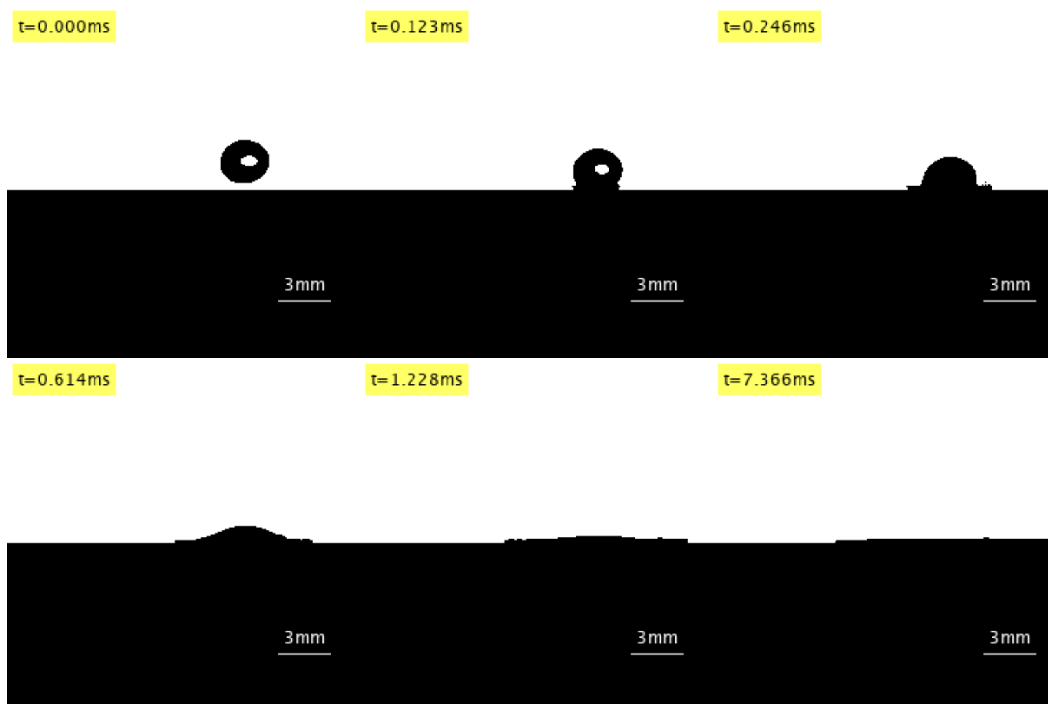


Figure 3.28: 4wt% impact onto nickel from 100cm.

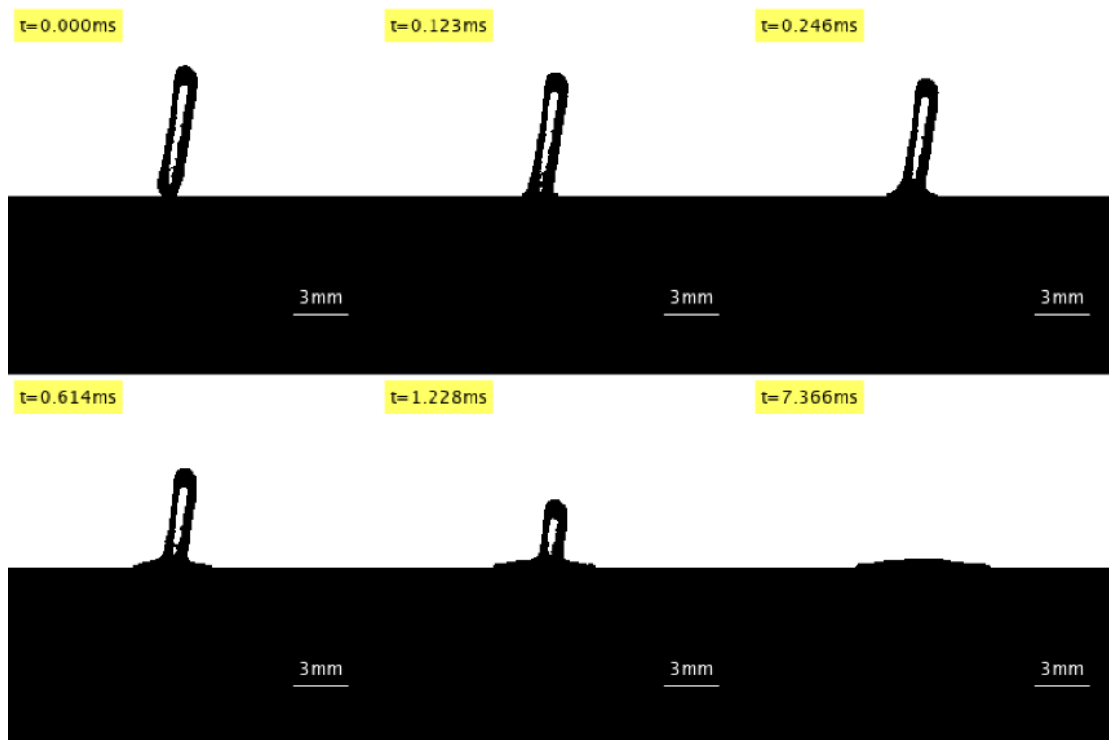


Figure 3.29: 6wt% impact onto nickel from 50cm.

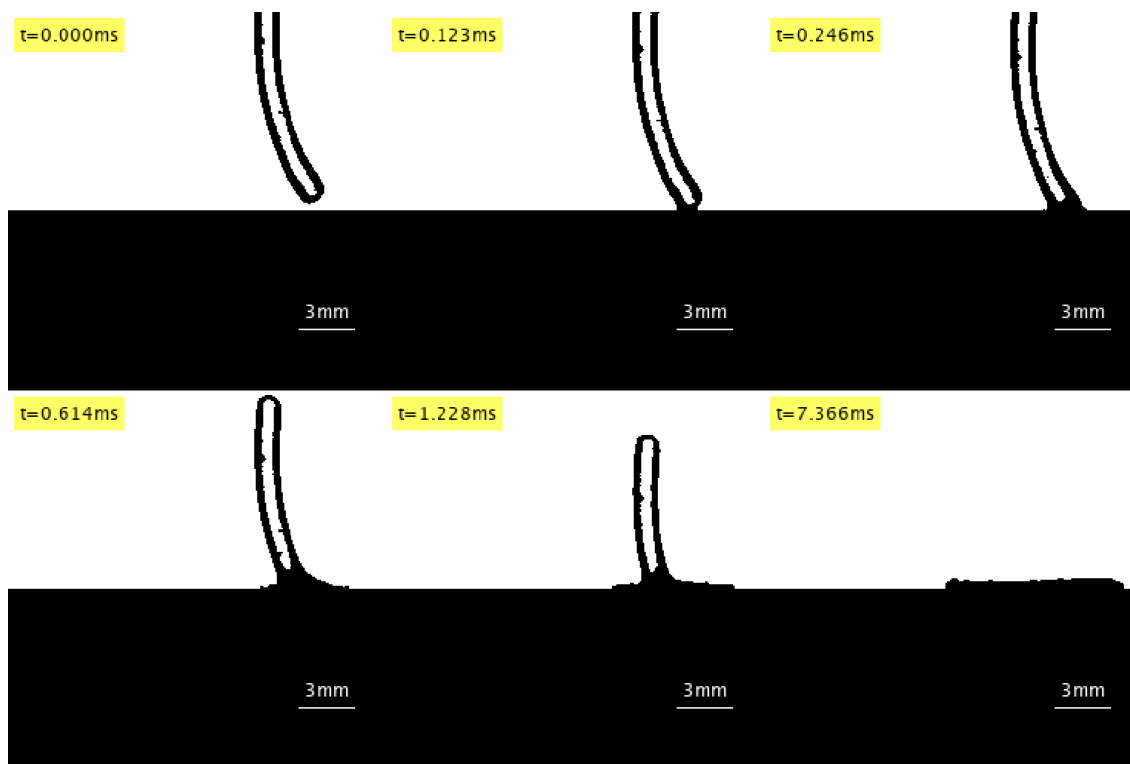


Figure 3.30: 6wt% impact onto nickel from 100cm.

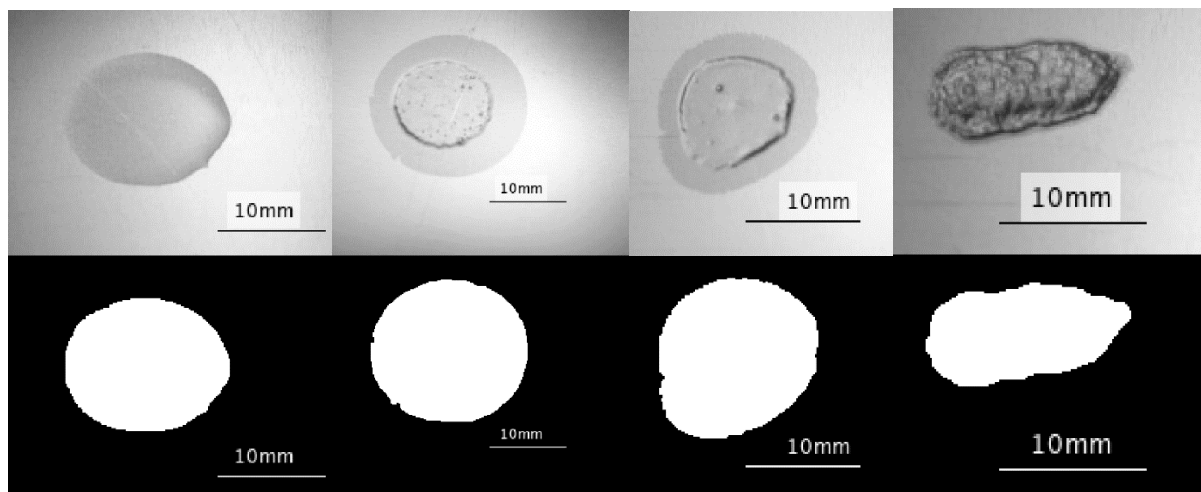


Figure 3.31: Spread comparison from 50cm onto nickel for 0wt% (left) to 6wt% (right).

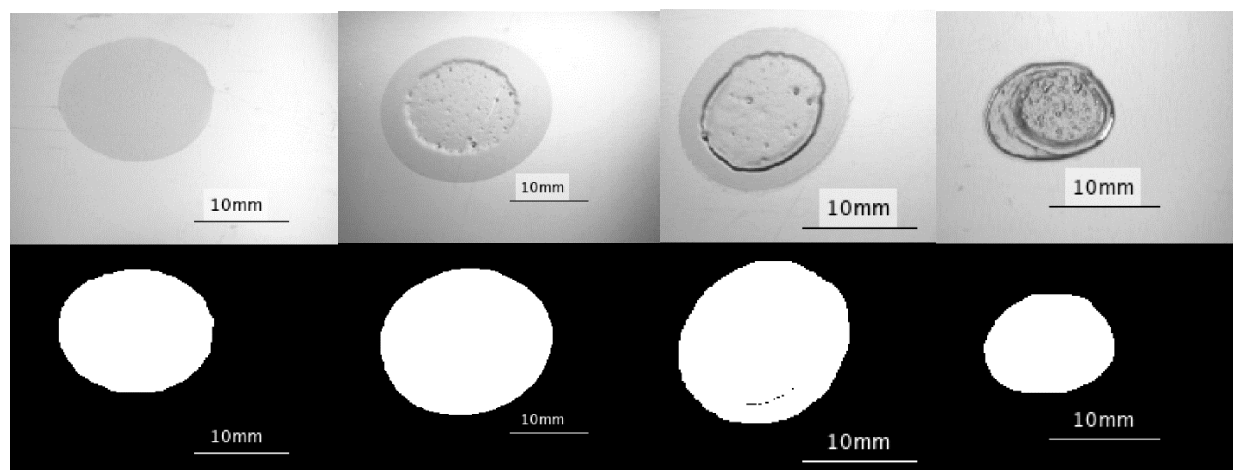


Figure 3.32: Spread comparison from 100cm onto nickel for 0wt% (left) to 6wt% (right).

Table 3.5: Impact characteristics from 50cm onto nickel.

Gellant Percentage	Volume (mm³)	Weber Number	Spread Diameter (mm)	Spread Area (mm²)	Reynolds Number
0wt%	12.06	0.79	14.80	60.62	3.373
2wt%	12.59	0.96	12.93	122.151	16.81
4wt%	9.66	0.96	11.38	62.39	0.5019
6wt%	20.84	0.88	7.56	29.07	0.04531

Table 3.6: Impact characteristics from 100cm onto nickel.

Gellant Percentage	Volume (mm³)	Weber Number	Spread Diameter (mm)	Spread Area (mm²)	Reynolds Number
0wt%	12.06	1.18	16.02	68.47	5.277
2wt%	13.68	1.38	15.53	129.91	33.01
4wt%	11.06	1.42	13.09	66.40	0.9289
6wt%	20.84	1.47	10.08	33.81	0.07490

These results are consistent with the previous as the 2wt% gel greatly increases the spread area, the 4wt% having comparable spread area as the 0wt%, and the 6wt% reducing the spread area by around half the spread of the 0wt%. This is an important note especially since the volume of the 6wt% droplet in the 100cm impact appears larger than the previous 6wt% drops. The average droplet size is still being used for the 6wt% due to the highly unpredictable nature of the droplet but appearing larger while still decreasing the spread area by such a large amount is promising for impacts which may involve larger amounts of fuel. The height increase effect also shows consistent results although it has a more noticeable affect for the 4wt% and 6wt% impacts when compared to the previous spread area which barely increase when the height was doubled. The dynamic spread plots are included in Figure 3.33.

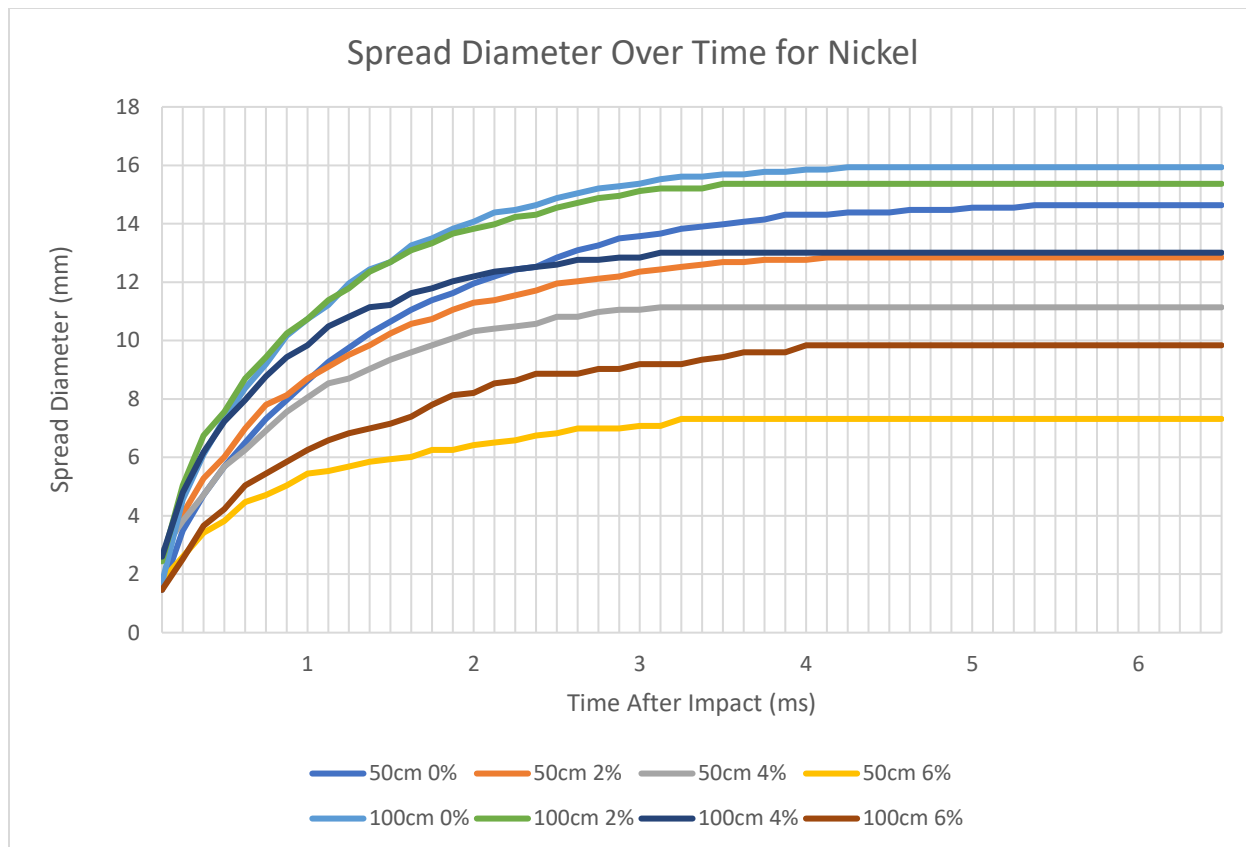


Figure 2.33: The spread diameter over time for each impact onto the nickel surface.

3.3.3 Stainless Steel

Again, the experiments were repeated but for the stainless-steel alloy. Figures 3.34-3.41 show the impact of each gel at both heights onto the stainless-steel plate, Figures 3.42-3.43 show the spread area from above, and Tables 3.6 and 3.7 display the key impact characteristics.

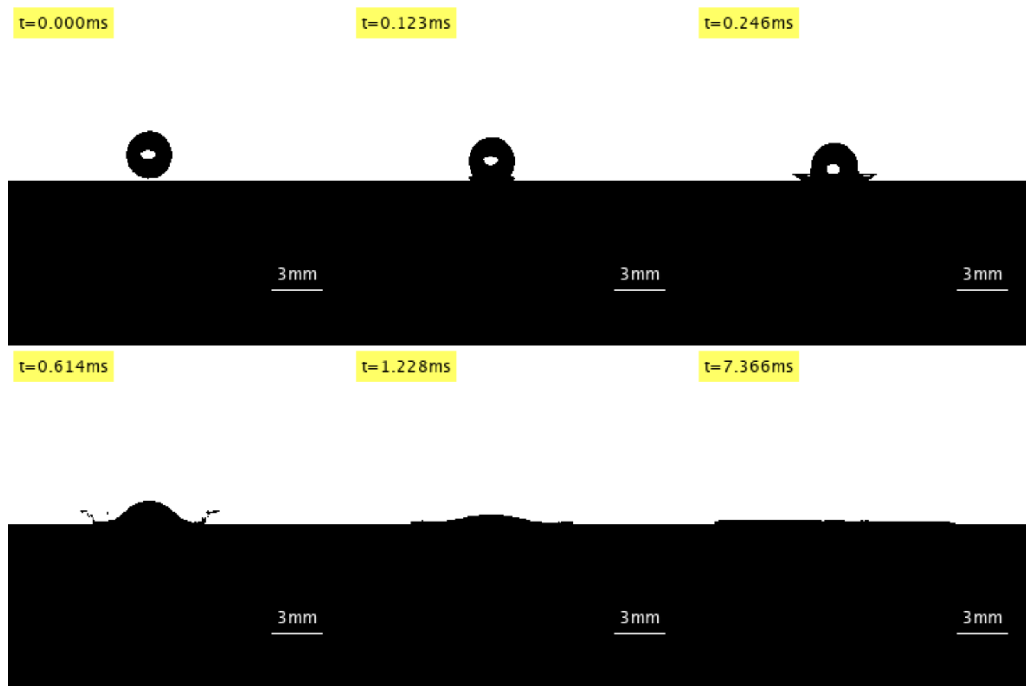


Figure 3.34: 0wt% impact onto stainless steel from 50cm.

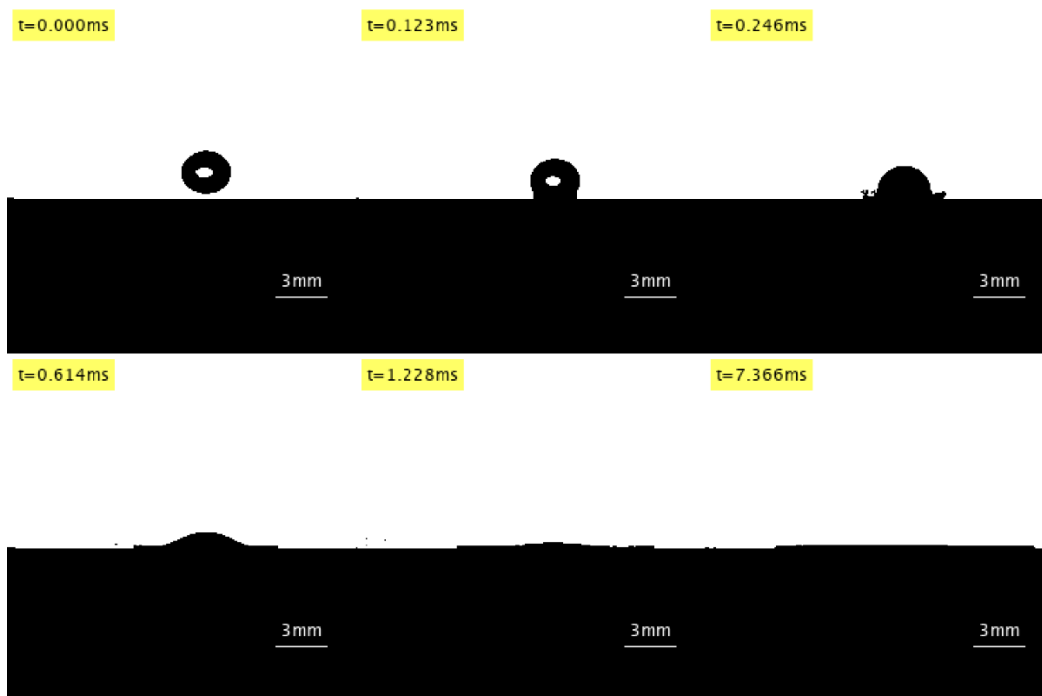


Figure 3.35: 0wt% impact onto stainless steel from 100cm.

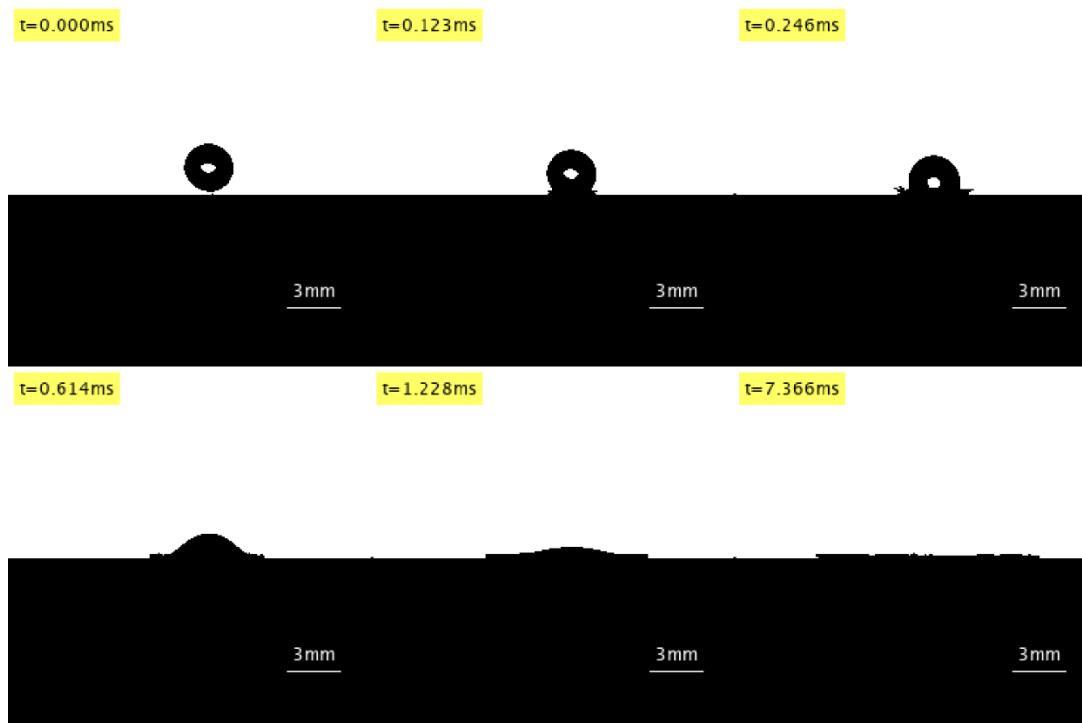


Figure 3.36: 2wt% impact onto stainless steel from 50cm.

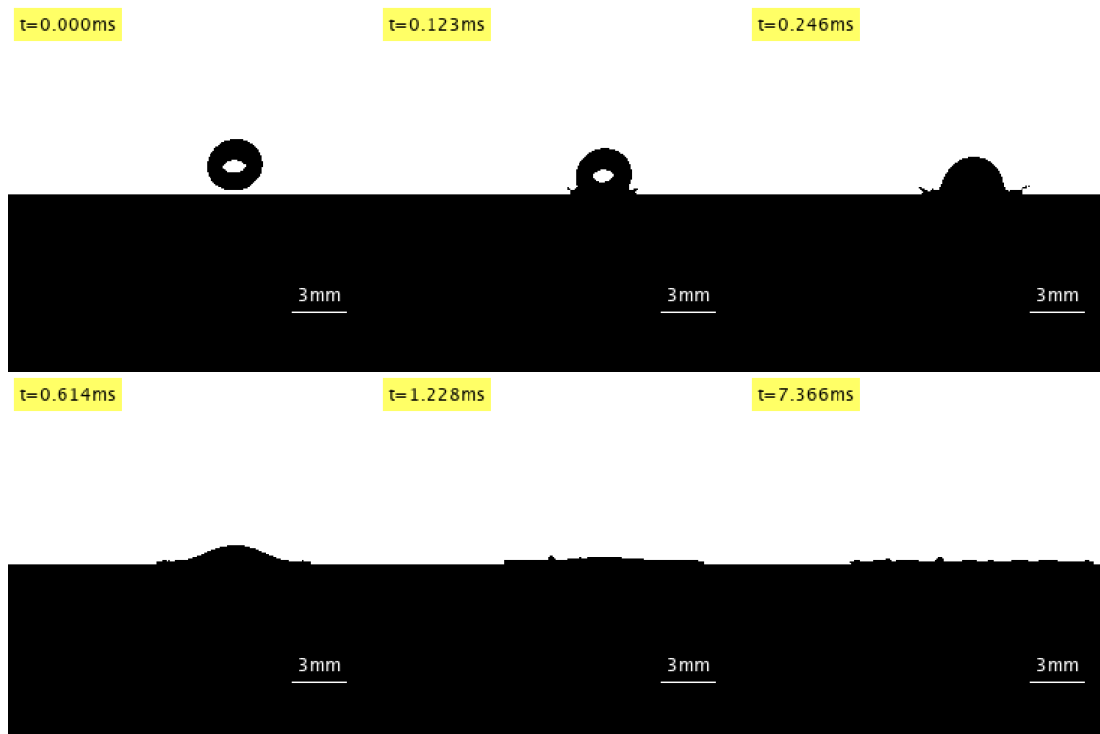


Figure 3.37: 2wt% impact onto stainless steel from 100cm.

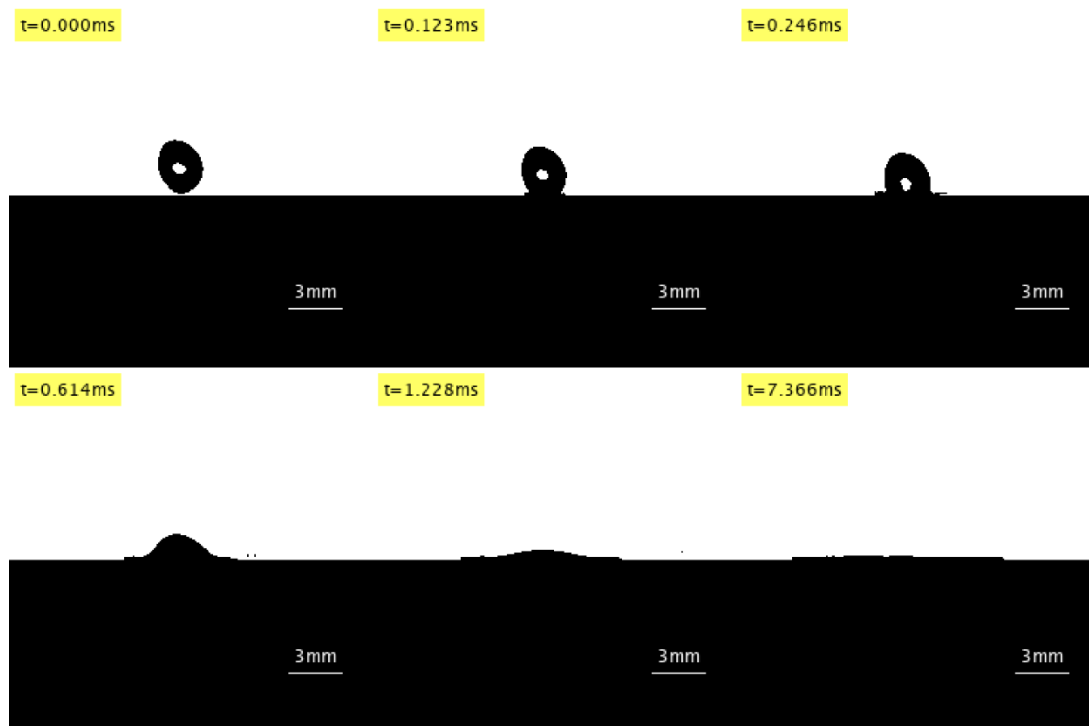


Figure 3.38: 4wt% impact onto stainless steel from 50cm.

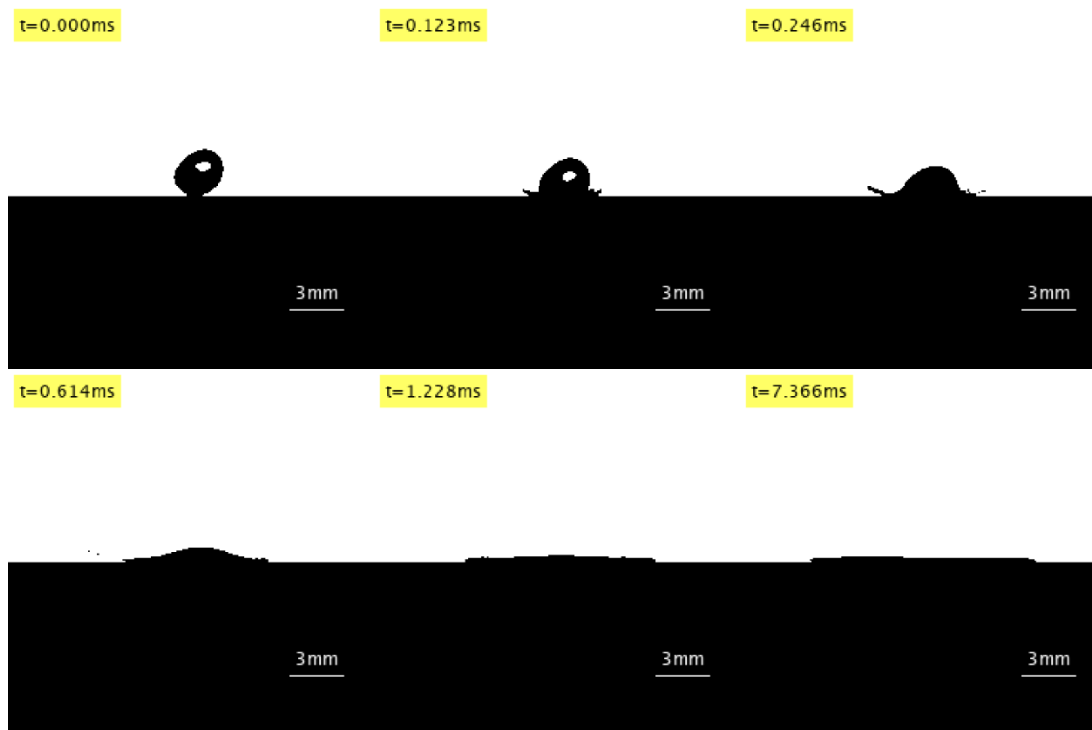


Figure 3.39: 4wt% impact onto stainless steel from 100cm.

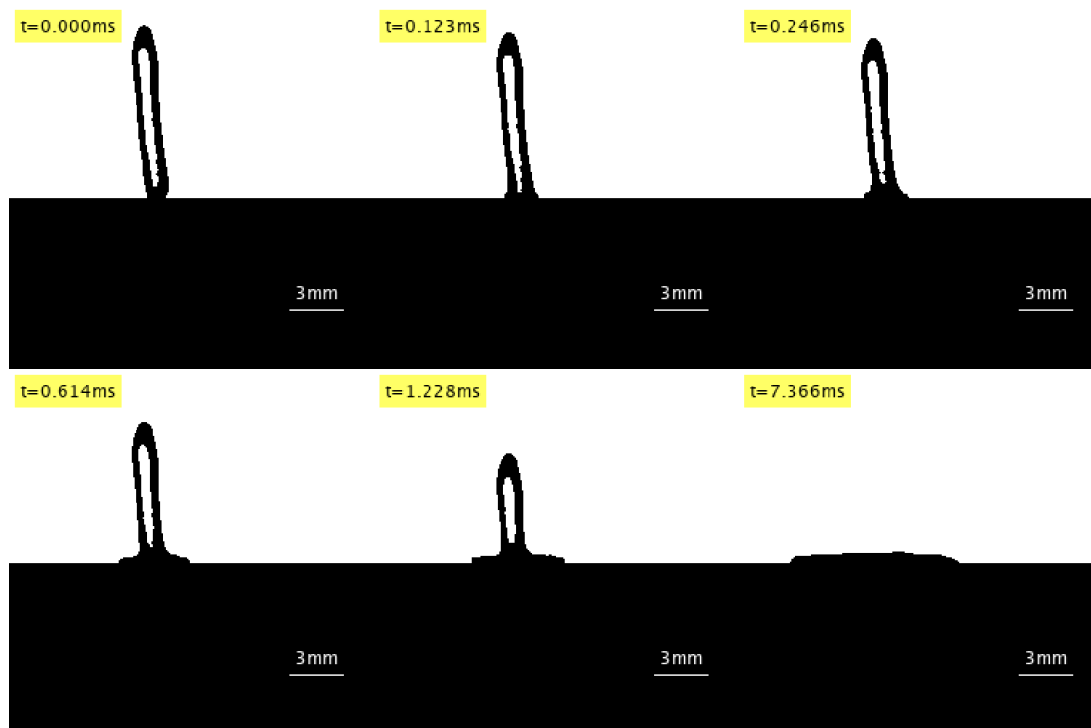


Figure 3.40: 6wt% impact onto stainless steel from 50cm.

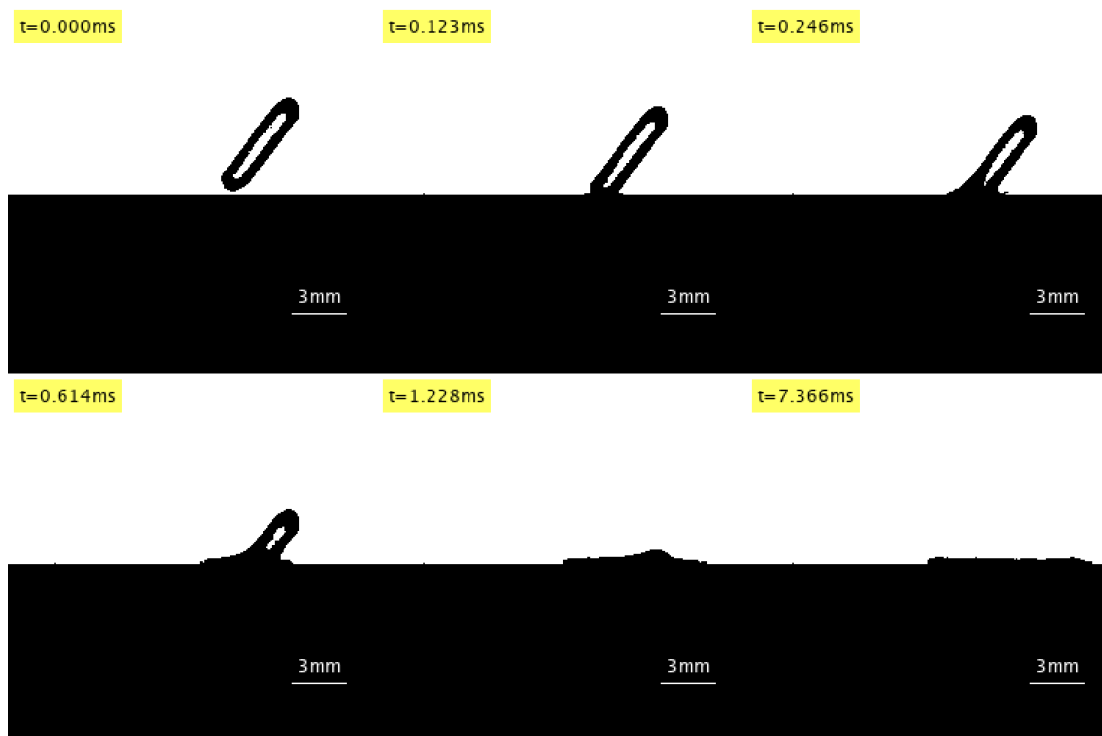


Figure 3.41: 6wt% impact onto stainless steel from 50cm.

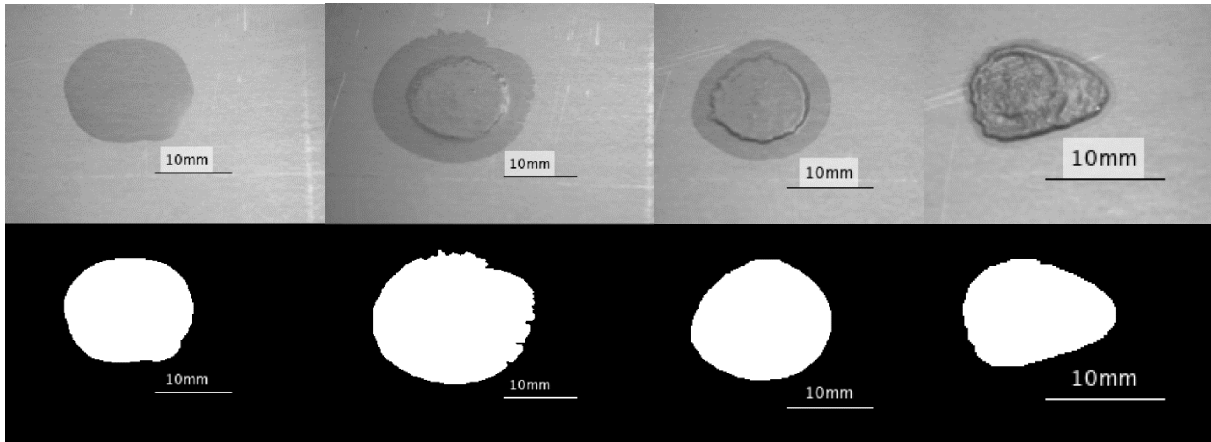


Figure 3.42: Spread comparison from 50cm onto stainless steel for 0wt% (left) to 6wt% (right).

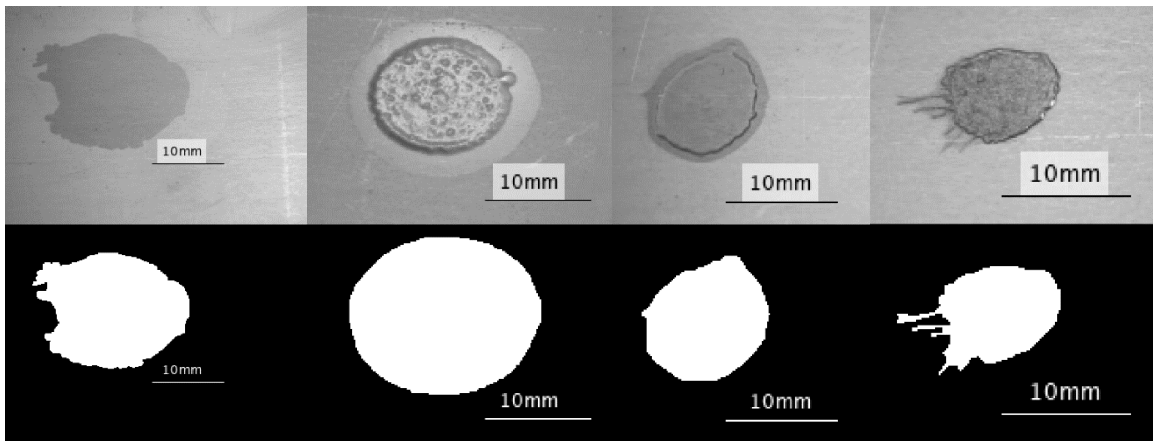


Figure 3.43: Spread comparison from 100cm onto stainless steel for 0wt% (left) to 6wt% (right).

Table 3.7: Impact characteristics from 50cm onto stainless steel.

Gellant Percentage	Volume (mm³)	Weber Number	Spread Diameter (mm)	Spread Area (mm²)	Reynolds Number
0wt%	12.06	0.79	14.63	75.60	3.373
2wt%	12.06	0.90	12.85	121.85	15.33
4wt%	12.06	0.97	12.03	70.13	0.5005
6wt%	20.84	0.86	9.59	34.68	0.04946

Table 3.8: Impact characteristics from 100cm onto stainless steel.

Gellant Percentage	Volume (mm³)	Weber Number	Spread Diameter (mm)	Spread Area (mm²)	Reynolds Number
0wt%	10.58	1.09	15.53	104.33	4.731
2wt%	14.84	1.43	13.66	85.96	35.24
4wt%	10.58	1.38	12.76	37.41	0.9283
6wt%	20.84	1.76	9.35	23.64	0.8657

These results are promising but not entirely consistent. What stands out the most is the surprisingly low value for the spread area of the 4wt% droplet from 100cm. This is around half of what was expected as it typically produces a spread area similar to or slightly smaller than that of the 0wt% gel. Due to the inner spread diameter being consistent with previous data, the anomalous behavior of this impact is the result of a much smaller outer area than usual. This is not much of an issue as long as the inner diameter is consistent because the outer spread area is not well understood and quite unpredictable. It is also noteworthy that the 6wt% droplet decreased the spread area by much more than it typically does in the 100cm impact, decreasing it by slightly more than a factor of four. This is difficult to explain but is likely the result of a combination of a larger than average spread area for the 0wt% impact and a lower-than-average spread area for the 6wt% impact. Again, the spread formation can be analyzed in Figure 3.44 with a plot of the spread diameters over time.

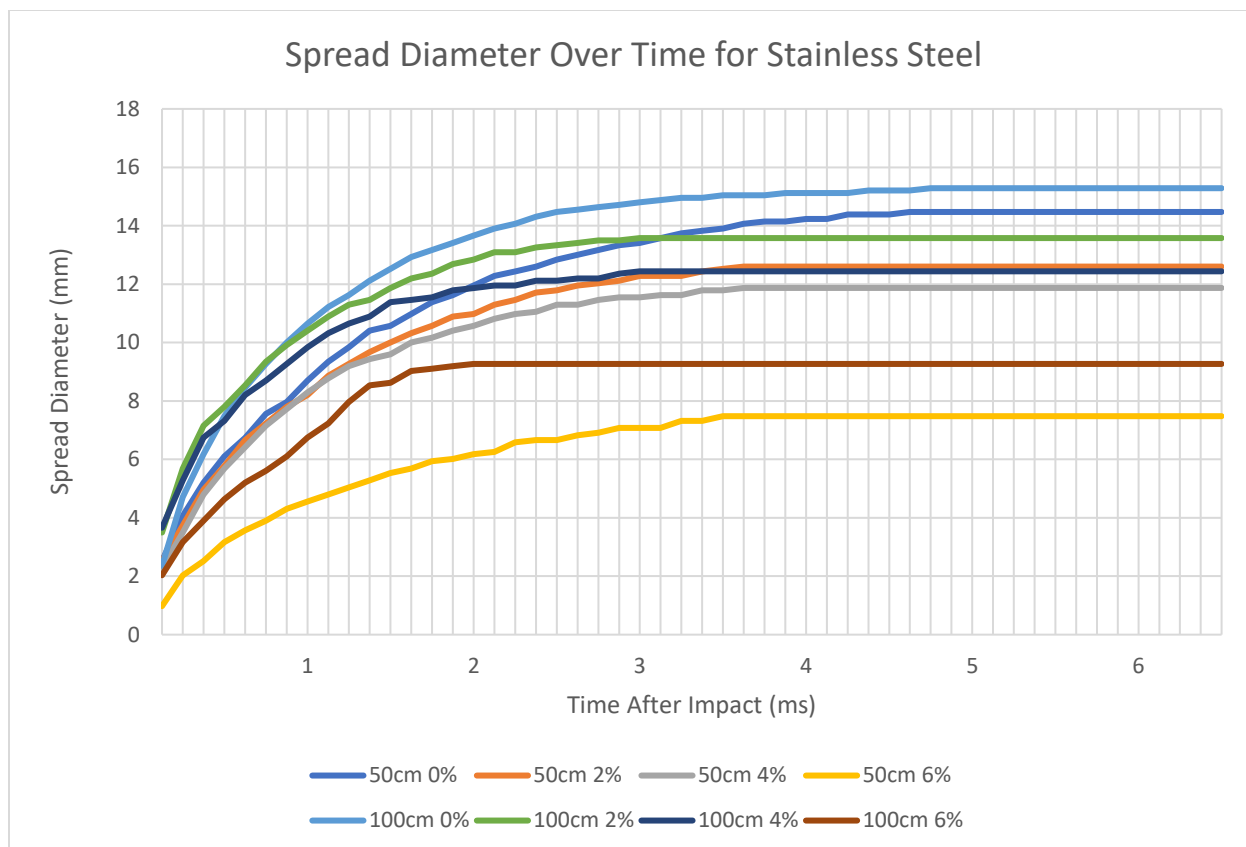


Figure 3.44: The spread diameter over time for each impact onto the stainless steel surface.

3.3.4 Smooth oleophobic glass

As stated before, the smooth glass was made oleophobic through the use of a surface coating. This results in a less than perfect oleophobic surface that will still provide a good comparison for the kerosene droplet tests. Again, Figures 3.45-3.52 show the droplets impacting the surface for each gel at each height, Figures 3.53-3.54 show the splash pattern from above, and Tables 3.8-3.9 display key impact characteristics.

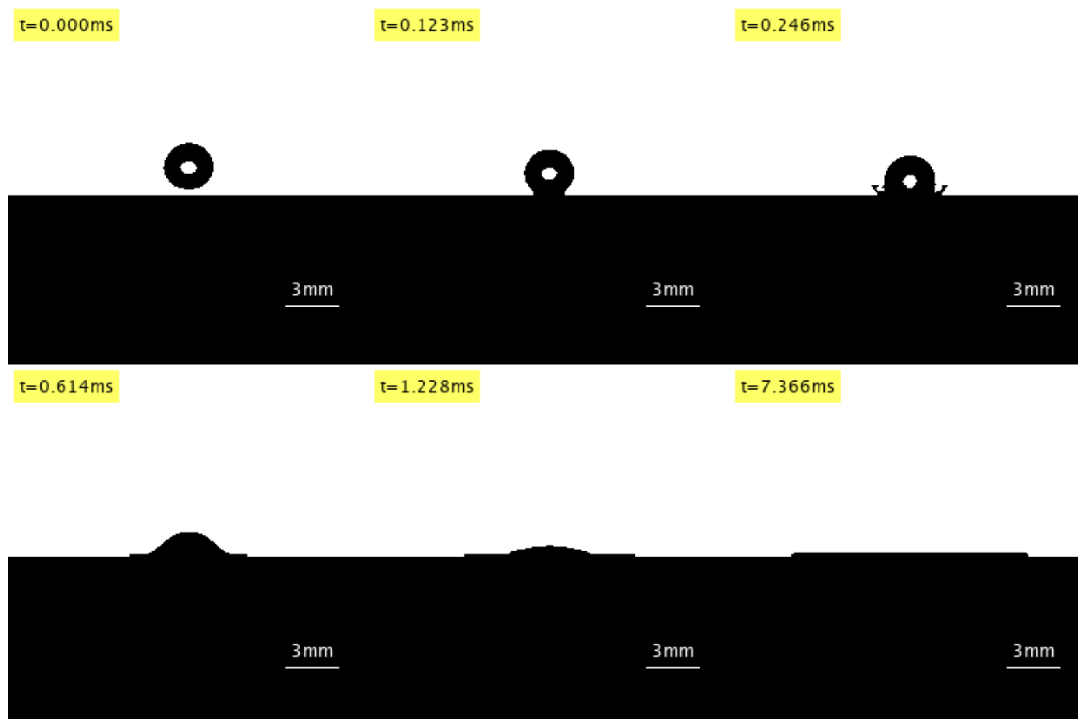


Figure 3.45: 0wt% impact onto smooth oleophobic glass from 50cm.

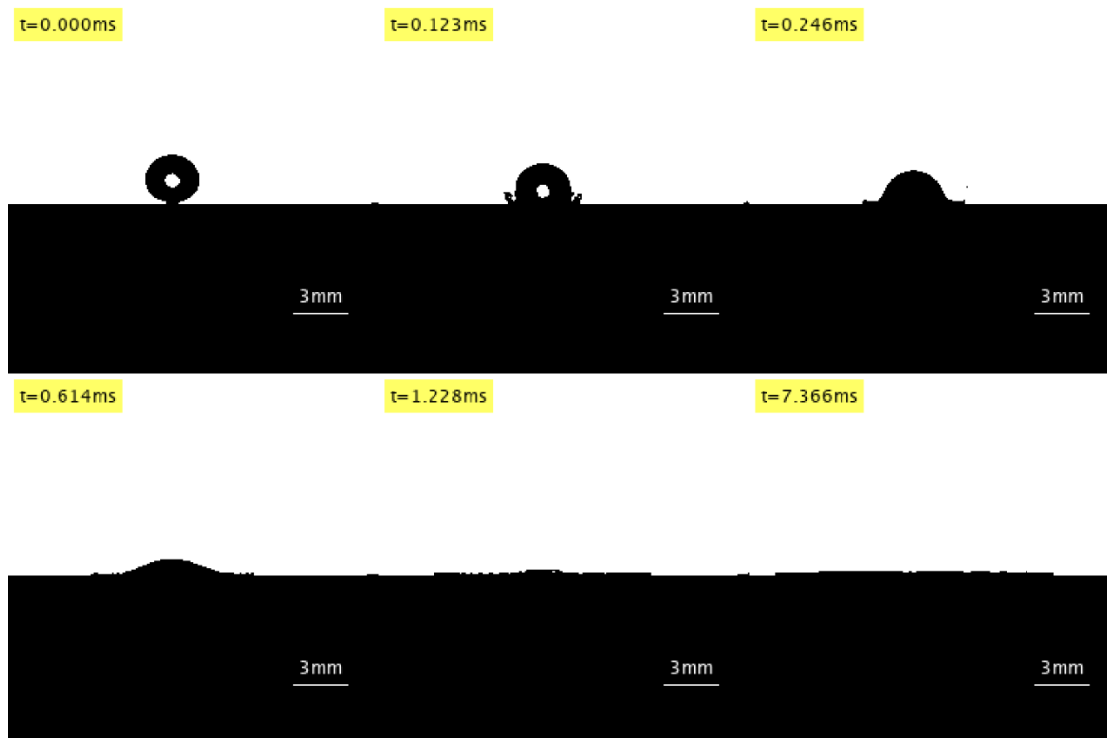


Figure 3.46: 0wt% impact onto smooth oleophobic glass from 100cm.

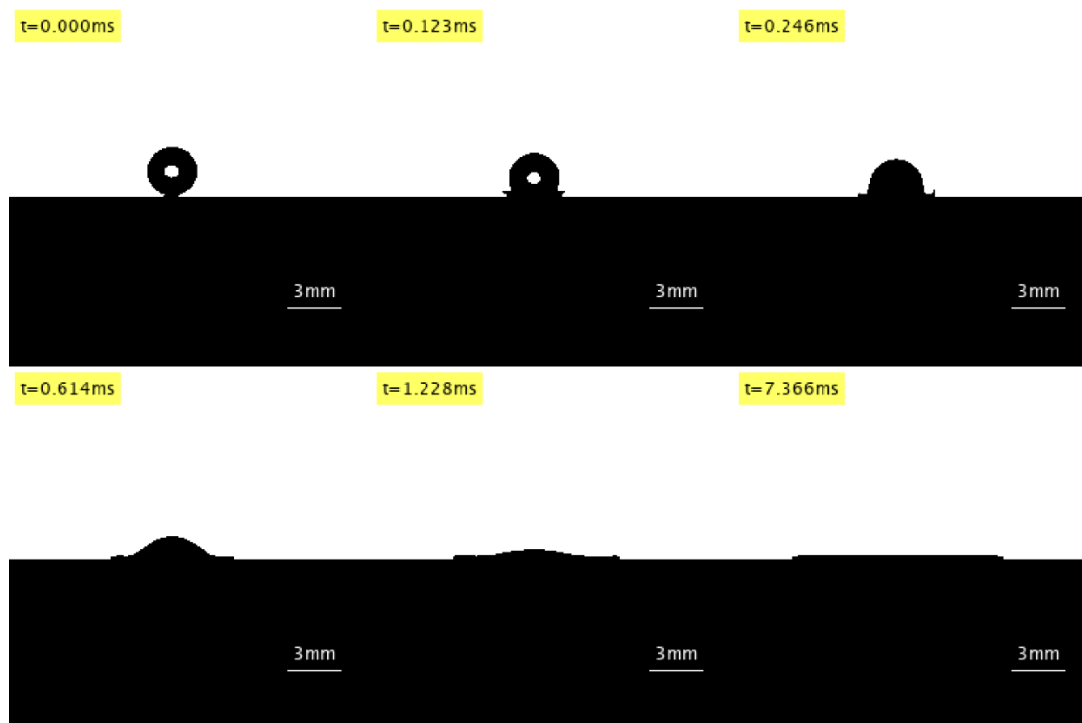


Figure 3.47: 2wt% impact onto smooth oleophobic glass from 50cm.

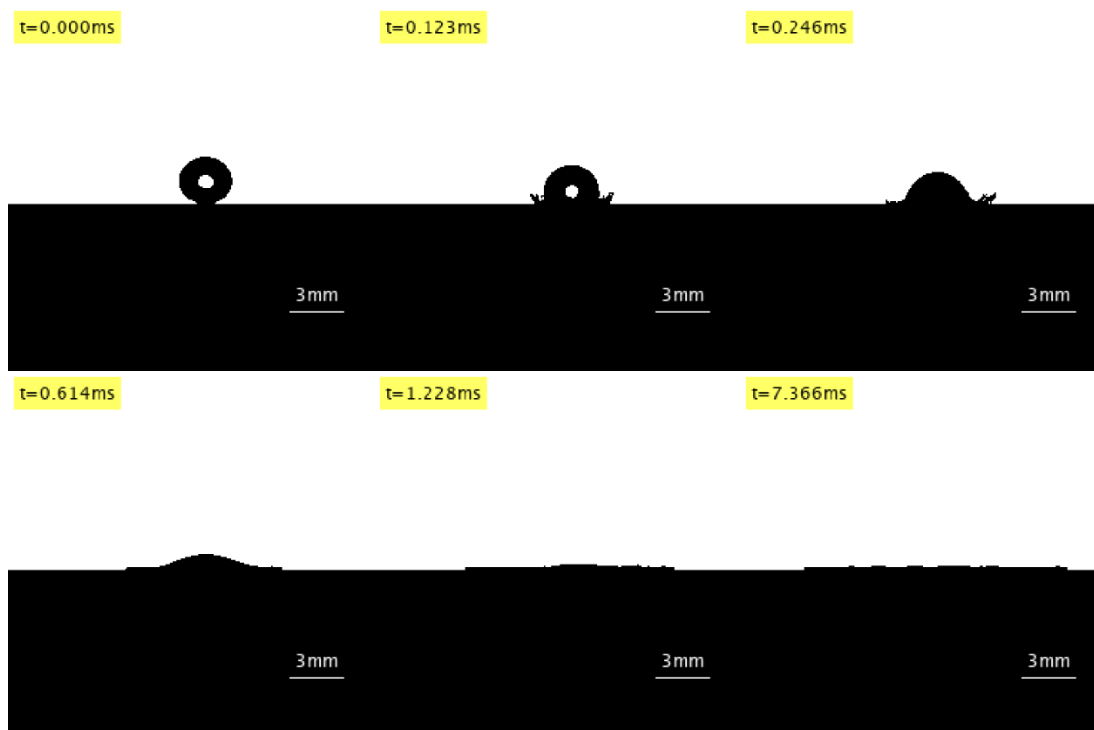


Figure 3.48: 2wt% impact onto smooth oleophobic glass from 100cm.

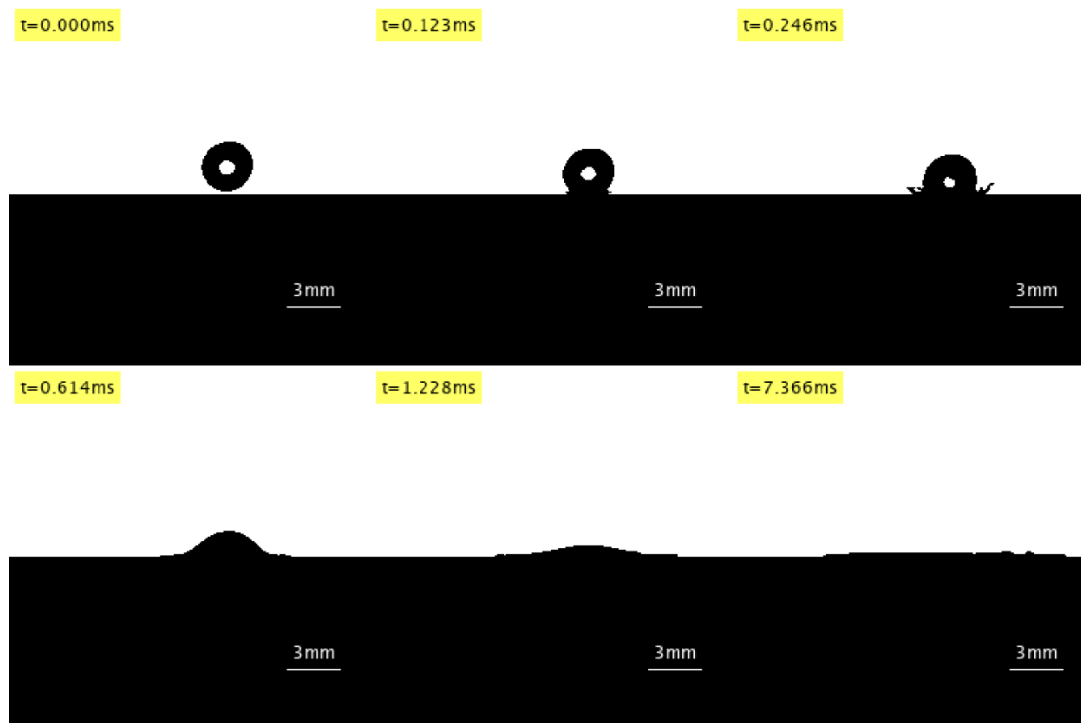


Figure 3.49: 4wt% impact onto smooth oleophobic glass from 50cm.

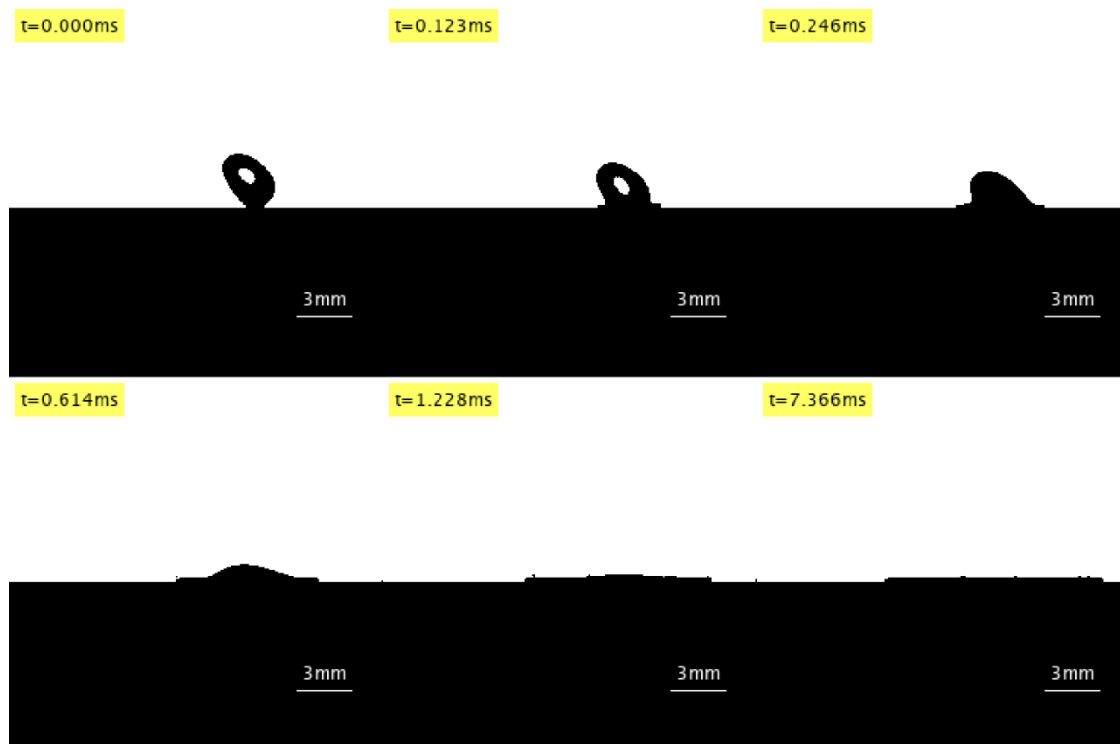


Figure 3.50: 4wt% impact onto smooth oleophobic glass from 100cm.

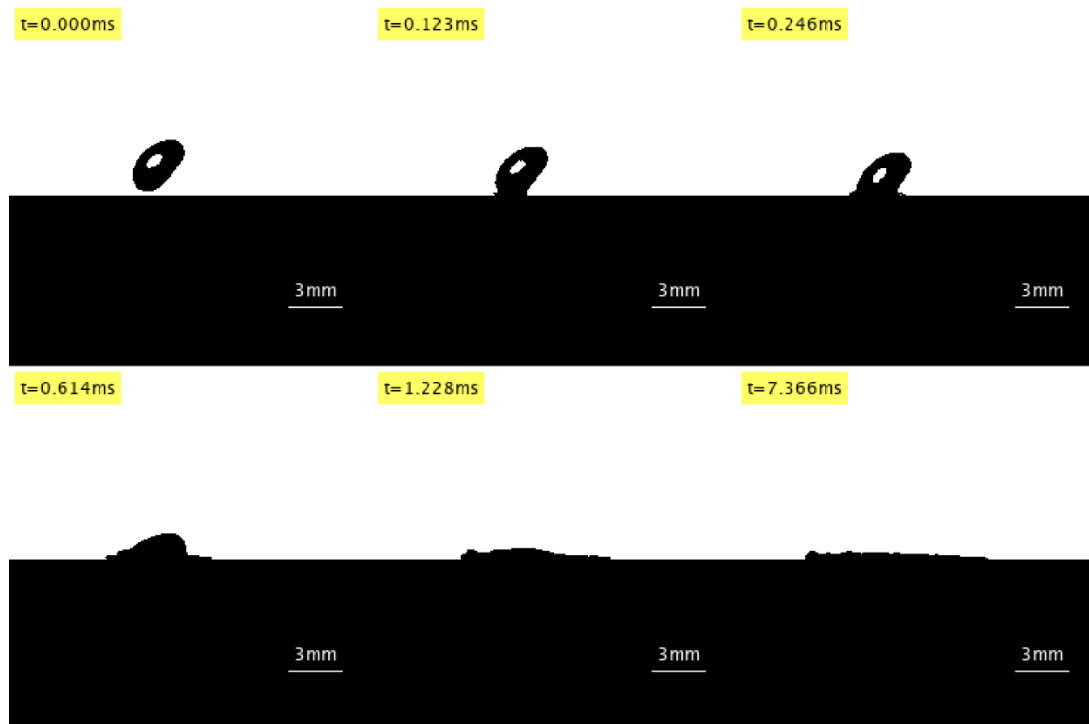


Figure 3.51: 6wt% impact onto smooth oleophobic glass from 50cm.

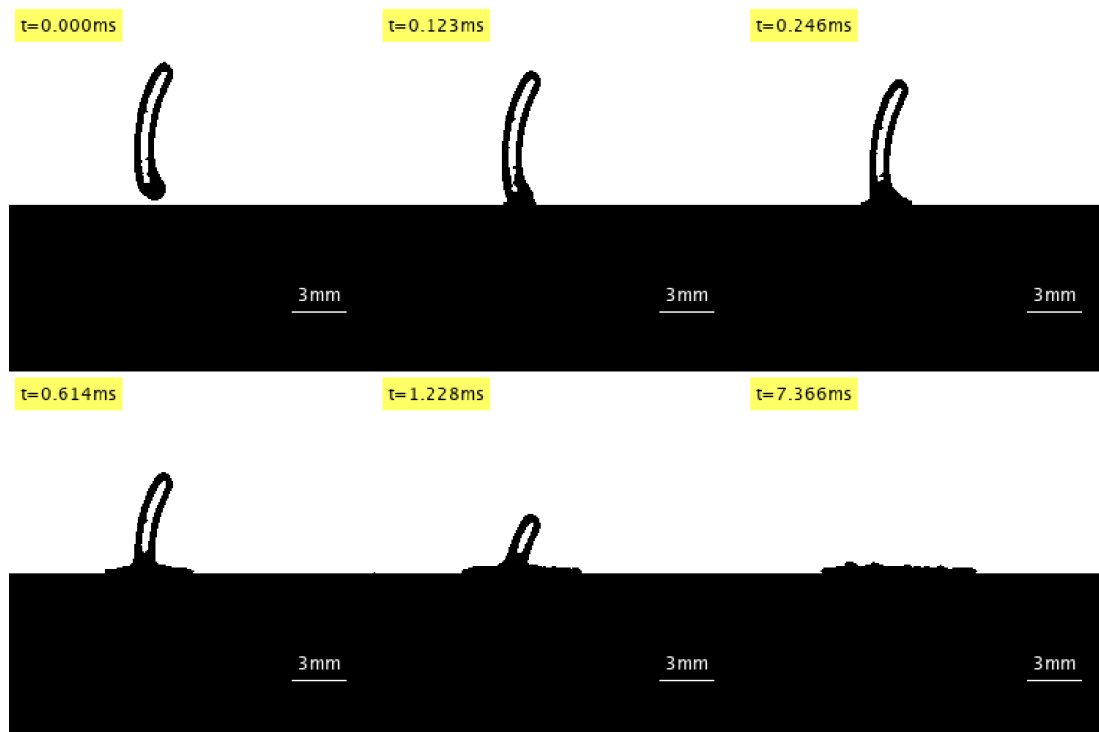


Figure 3.52: 6wt% impact onto smooth oleophobic glass from 100cm.

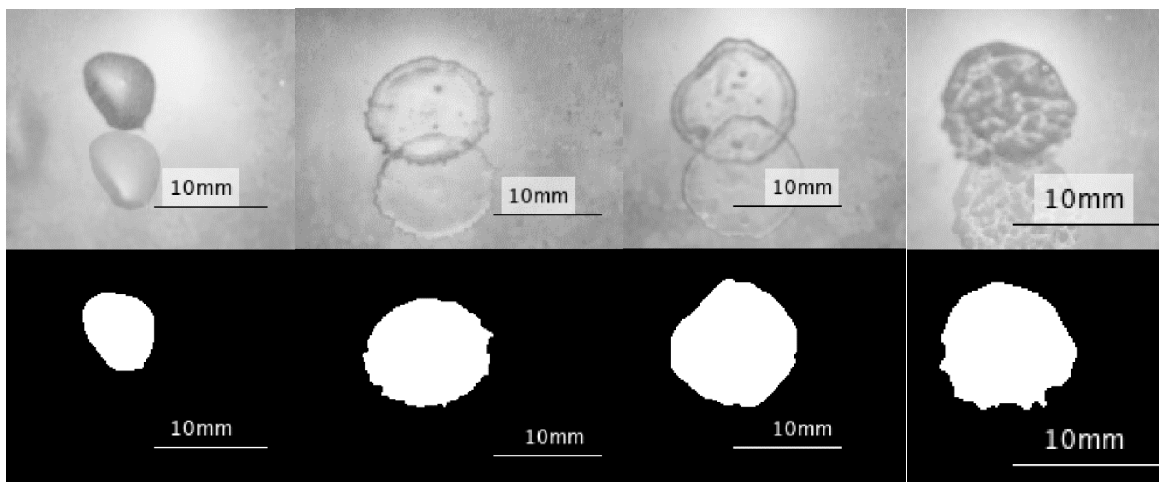


Figure 3.53: Spread comparison from 50cm onto oleophobic smooth glass for 0wt% (left) to 6wt% (right).

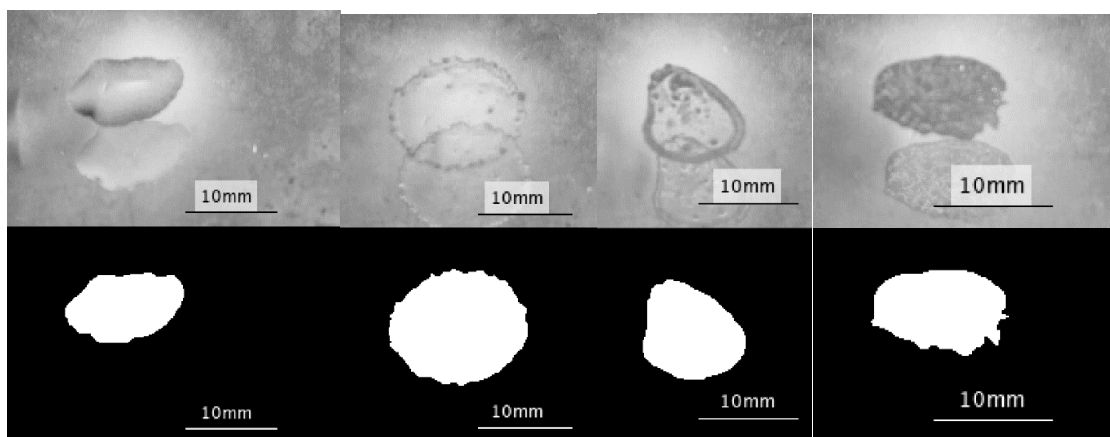


Figure 3.54: Spread comparison from 100cm onto oleophobic smooth glass for 0wt% (left) to 6wt% (right).

Table 3.9: Impact characteristics from 50cm onto oleophobic smooth glass.

Gellant Percentage	Volume (mm³)	Weber Number	Spread Diameter (mm)	Spread Area (mm²)	Reynolds Number
0wt%	11.56	0.76	13.9	13.87	3.306
2wt%	12.06	0.99	12.20	36.35	18.32
4wt%	13.68	1.06	13.82	40.55	0.5014
6wt%	20.84	1.05	10.08	24.37	0.04550

Table 3.10: Impact characteristics from 100cm onto oleophobic smooth glass.

Gellant Percentage	Volume (mm³)	Weber Number	Spread Diameter (mm)	Spread Area (mm²)	Reynolds Number
0wt%	12.06	1.12	15.69	29.92	4.9856
2wt%	12.59	1.32	15.04	55.21	30.92
4wt%	13.68	1.42	12.03	30.66	0.9289
6wt%	20.84	1.19	8.70	24.90	0.08031

Based on these results, the oleophobic surface coating has a strong effect on the spread area, specifically for the lower gelling percentage. The pure kerosene in particular experiences the most spread decrease when compared to the smooth glass impact. Additionally, the oleophobic coating reduced the surface area by eliminating the outer ring that appeared in the 2wt% and 4wt% gels. It even had a relatively strong effect on the 6wt% gel reducing its spread area by almost 10mm²s for both the 50cm and 100cm impacts when compared to the smooth glass. Along with this, there is no significant change in spread diameter leading to the conclusion that there is recession in the lower wt% gels where they initially rapidly expand to a particular diameter before slowly receding due surface forces. This is not captured in the high-speed video due to the large time scale of the recession. For comparison, the initial spread occurs in just a few milliseconds while the subsequent recession was observed to take several seconds to conclude. Again, the initial spread can be seen in the spread diameter over time plot in Figure 3.55. The initial spread does not seem to be stunted for the oleophobic glass when compared to the smooth glass surface from Figure 3.11.

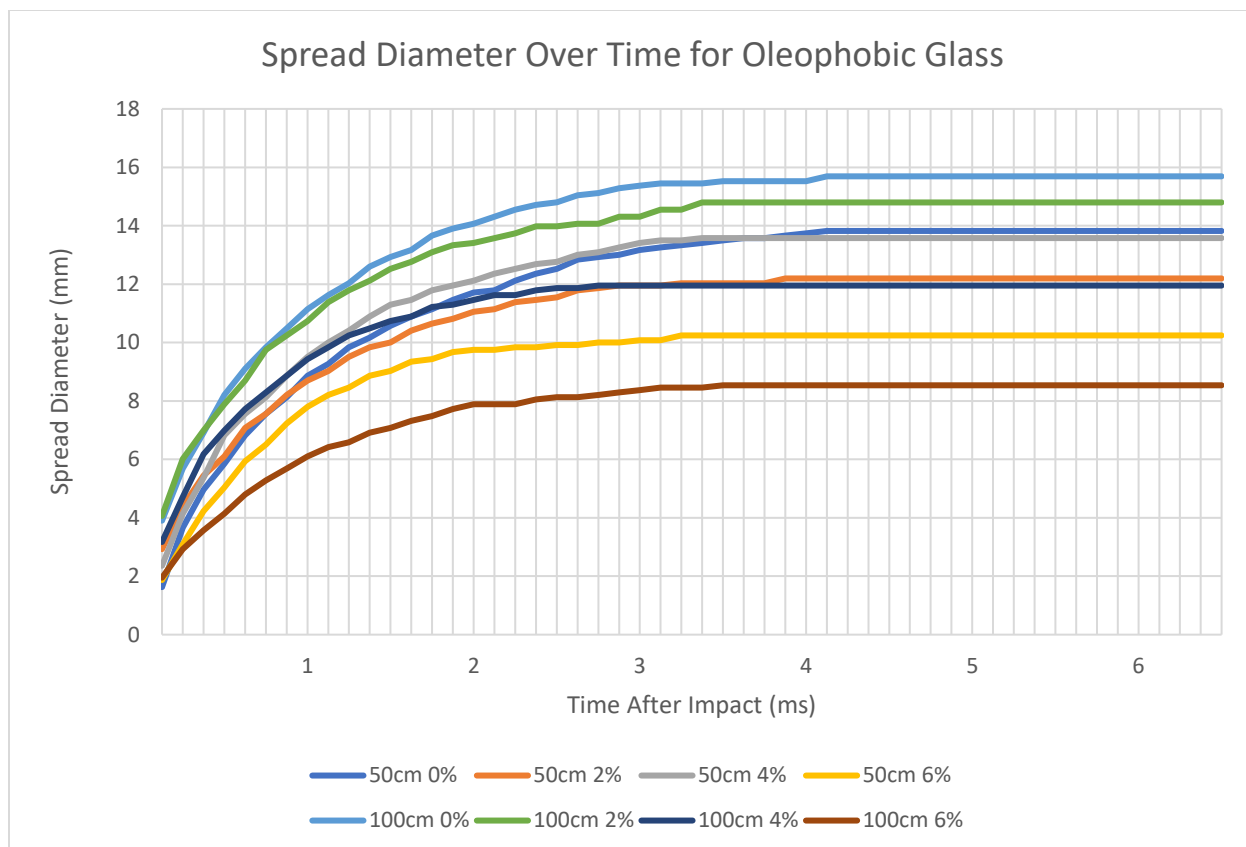


Figure 4.55: The spread diameter over time for each impact onto the oleophobic glass surface.

3.4 Next steps

Although some results seem conclusive, there is still a wide array of topics that should be explored to determine more about the impact characteristics of these gels. For example, using a naturally oleophobic surface would be more consistent than using a surface coating which is not entirely oleophobic and may degrade over time. More analysis can be done to explore consistent contact angle measurements as well as quantifying the elasticity of each gel. Along with this, a wider range of drop heights would give a better idea of how the spread area increases with the Weber number. However, increasing the height comes with its own problems including stability of the setup and consistency in drop location. Instead of increasing the height to increase the

velocity of each drop, it is currently being considered to instead change the speed of the impact plate. This introduces issues mainly involving synching the plate and droplet timing so that the impact occurs in the camera frame. A more practical experiment involving a moving plate would be to have the droplet impact a surface that is moving horizontally. This would mimic the impact characteristics of a droplet with more dynamic motion. Additionally, to explore the formation of the outer spread area, the DSLR camera can be replaced by a high speed camera. This would allow for plots of the spread diameter over time for a much longer time scale giving insight into the outer spread formation. Finally, exploring the atomization properties of these gels would be worth researching as this is often a limiting factor when considering the usage of gelled fuels.

CHAPTER 4

CONCLUSION

The control variables involved in these tests had a range of effects on the impact characteristics of the fluids. On average, the addition of fumed silica as a gelling agent at 2wt% increases the spread area of the impact significantly. This was unexpected as it was postulated that any increase in gelling agent in the mixture would result in a subsequent decrease in spread area. This is not the case as the outer spread area generally did not see a decrease until the percentage of fumed silica in the mixture increased beyond 4wt%. However, beyond this point the spread area decreased by a large margin as seen in the 6wt% droplet impacts despite their much larger average volume. On the contrary, the inner spread diameter showed expected results throughout all the experiments, decreasing as the gellant percentage increased. The height change from 50cm to 100cm increased the Weber number for each impact resulting in only a slightly larger average spread area. This had a stronger effect on the lower wt% gels while hardly affecting the 6wt% gel at all. Additionally, the surfaces displayed slightly different impact characteristics. Each metal surface showed relatively similar, consistent results with the exception of some of the 4wt% drops likely due to the unpredictability of the outer spread area development. The smooth oleophobic glass surface had the most outlying impact characteristics of all the surface, dramatically decreasing the spread area for the lower wt% gels as well as removing the outer spread ring that consistently occurred on the 2wt% and 4wt% gels. Overall, these droplet impact experiments showed promising results for gels with higher gellant percentages which reduced the spread area significantly.

REFERENCES

- Cao, Q., Liao, W., Natan, B., Feng, F., & Wu, W. (2022). Secondary atomization of non-Newtonian kerosene gel at low Weber numbers: A numerical study. *Aerospace Science and Technology*, 120.
- Cao, Q., Liao, W., Wu, W., & Feng, F. (2019). Combustion characteristics of inorganic kerosene gel droplet with fumed silica as gellant. *Experimental Thermal and Fluid Science*. 103, 377-384.
- Jadidbonab, H., Malgarinos, I., Karathanassis, I., Mitroglou, N., & Gavaises, M., (2018). We-T classification of diesel fuel droplet impact regimes. *Proceedings of the Royal Society A: Mathematical, Physical, and Engineering Sciences*. 474(2215).
- Fu, Q., Ge, F., Wang, W., & Yang, L. (2019). Spray characteristics of gel propellants in an open-end swirl injector. *Fuel*. 254.
- Jørgensen, L., Merrer, M.L., Delanoe^o-Ayaria, H., & Barentinab, C. (2015). Yield stress and elasticity influence on surface tension measurements. *Soft Matter*. 11.
- Li, J., Ma, H., Li, Y., Yang, Z., He, G., & Wang, B. (2022a). The micromorphology and large amplitude oscillatory shear behaviors of hydrocarbon gel fuels filled with fumed silica and aluminum sub-microparticles. *Colloids and Surfaces A: Physicochemical and Engineering Aspects*. 654.
- Li, M., Wu, Y., Cao, Q., Yuan, X., Chen, X., Han, J., & Wu, W. (2022b). Rheological Properties of Organic Kerosene Gel Fuel. *Gels*. 8(8).
- Luu, L. & Forterre, Y. (2009). Drop impact on yield-stress fluids. *Journal of Fluid Mechanics*, 632, 301-327.

- Padwal, M.B., & Mishra, D.P. (2013). Synthesis of Jet A1 gel fuel and its characterization for propulsion applications. *Fuel Processing Technology*. 106, 359-365.
- Padwal, M.B., Natan, B., & Mishra, D.P., (2021). Gel propellants. *Progress in Energy and Combustion Science*, 83.
- Wang, Y., Gratadeix, A., Do-Quang, M., & Amberg, G. (2016). Events and conditions in droplet impact: A phase field prediction. *International Journal of Multiphase Flow*. 84, 54-65.
- Yang, D., Xia, Z., Huang, L., Ma, L., Chen, B., & Feng, Y. (2020). Synthesis of metallized kerosene gel and its characterization for propulsion applications. *Fuel*. 262.